

Annual Review of Physical Chemistry

Spatially Resolved Photogenerated Exciton and Charge Transport in Emerging Semiconductors

Naomi S. Ginsberg^{1,2,3} and William A. Tisdale⁴

¹Department of Chemistry and Department of Physics, University of California, Berkeley, California 94720, USA; email: nsginsberg@berkeley.edu

²Material Sciences Division and Molecular Biophysics and Integrated Bioimaging Division, Lawrence Berkeley National Laboratory, Berkeley, California 94720, USA

³Kavli Energy NanoSciences Institute, Berkeley, California 94720, USA

⁴Department of Chemical Engineering, Massachusetts Institute of Technology, Cambridge, Massachusetts 02139, USA; email: tisdale@mit.edu

Annu. Rev. Phys. Chem. 2020. 71:1–30

First published as a Review in Advance on
November 22, 2019

The *Annual Review of Physical Chemistry* is online at
physchem.annualreviews.org

<https://doi.org/10.1146/annurev-physchem-052516-050703>

Copyright © 2020 by Annual Reviews.
All rights reserved

Keywords

heterogeneous energy materials, nonequilibrium dynamics, optical spectroscopy, spatiotemporal, diffusion, ultrafast microscopy

Abstract

We review recent advances in the characterization of electronic forms of energy transport in emerging semiconductors. The approaches described all temporally and spatially resolve the evolution of initially localized populations of photogenerated excitons or charge carriers. We first provide a comprehensive background for describing the physical origin and nature of electronic energy transport both microscopically and from the perspective of the observer. We introduce the new family of far-field, time-resolved optical microscopies developed to directly resolve not only the extent of this transport but also its potentially temporally and spatially dependent rate. We review a representation of examples from the recent literature, including investigation of energy flow in colloidal quantum dot solids, organic semiconductors, organic-inorganic metal halide perovskites, and 2D transition metal dichalcogenides. These examples illustrate how traditional parameters like diffusivity are applicable only within limited spatiotemporal ranges and how the techniques at the core of this review,

ANNUAL
REVIEWS **CONNECT**

www.annualreviews.org

- Download figures
- Navigate cited references
- Keyword search
- Explore related articles
- Share via email or social media

especially when taken together, are revealing a more complete picture of the spatiotemporal evolution of energy transport in complex semiconductors, even as a function of their structural heterogeneities.

1. INTRODUCTION

One of the most important properties of semiconductors is their ability to transport electronic energy. This energy can take different forms: typically, free charges or neutral excitons, the latter being bound electron-hole pairs. Many scientists would like to explain the relationship between the interatomic- or intermolecular-level structure of a material and its ability to transport energy. Why are some materials highly effective while others are not? How do the ways that a material's basic building blocks configure themselves affect not only their strength or flexibility but also their electronic properties?

In some cases these questions can be answered through bulk band structure calculations and Hall effect (1–4), microwave conductivity (5–8), ultrafast optical or terahertz spectroscopy (9–14), cathodoluminescence (15, 16), or photoluminescence (PL) measurements (17–26). In many emergent electronic or optoelectronic semiconducting materials, such as those used to transduce light energy to electricity or vice versa, those bulk approaches do not accurately answer these questions because the materials are not homogeneous. A bulk continuum description may fail because of structural defects or other forms of disorder or because the material is not macroscopic in all spatial dimensions. The material, itself, may also be composed of multiple individual material components, where the interfaces between components dictate its electronic properties at least as much as transport within the components. At the other extreme, detailed measurements are made of energy flow in isolated components of a material, for example, proteins isolated from a photosynthetic membrane (27–30) or colloidal quantum dots (QDs) (31–33), yet these studies cannot on their own establish how the interconnections among components affect energy transport. A more complete description of how intermolecular or interparticle interactions and their variations determine the emergent energy transport properties of materials stands therefore to broadly impact both basic science and virtually all modern electronic and optoelectronic technologies.

Recently, photogenerated energy transport has begun to be characterized in ways that acknowledge the potential influence of structural inhomogeneities by optically observing the spatiotemporal evolution of photogenerated energy carriers in materials (34–41). This review focuses on the discoveries that have been made by employing such approaches and extrapolates to generalize what discoveries are in principle possible in the future as such approaches become more broadly employed. For example, exciton and charge transport have been spatially resolved to yield new insights in organic semiconductors (36, 42–46), composite QD solids (34, 47), hybrid organic-inorganic perovskites (36, 39, 48–52), 2D materials (40, 41, 53), and more traditional inorganic semiconductors (54). We and others have even discovered that new formalisms, beyond a standard diffusive picture, are required to describe transport (34, 37, 39). These discoveries have been made using innovations in time-resolved, or transient, photoluminescence (TRPL) (35, 44), transient absorption (TA) (38, 45), and transient scattering (TS) (36), each of which uses some form of optical imaging. Together, these innovations are beginning to change the way we view the fundamental process of energy transport and how it emerges from the microscopic properties of materials.

PL:
photoluminescence

QD: quantum dot

TRPL: time-resolved,
or transient,
photoluminescence

TA:
transient absorption

TS:
transient scattering

2. SPATIOTEMPORAL MEASUREMENTS OF PHOTOGENERATED ELECTRONIC ENERGY FLOW

Before describing how spatiotemporal characterization provides a more complete picture of energy flow in materials, we provide background on the microscopic physical underpinnings of electronic energy transport (Section 2.1), the three main optical spatiotemporal measurement techniques developed to resolve it (Section 2.2), and the formalism typically used to interpret data and relate it back to its microscopic origins (Section 2.3).

2.1. Energy Flow in Materials from a Microscopic Perspective

We begin by describing the fundamental nature of energy flow and how it arises from the physical and electronic properties of a material (55–57). In emerging semiconductors, in particular, which have more complex physical structures than traditional inorganic counterparts such as silicon, the microscopic interactions between individual building blocks (atoms, molecules, or nanocrystals and their ligands) critically affect the nature of energy transport through the way in which they determine the electronic structure of the material.

We first establish the vocabulary of photoinduced excitations in semiconductors. In all semiconductors, electronic states are typically categorized as being in either the valence (occupied) or conduction (unoccupied) bands, which are separated by an energy gap devoid of states. Photon absorption at energies greater than or equal to the size of this so-called band gap promotes an electron to the conduction band, leaving behind a so-called hole in the valence band—an effective, positively charged particle. As shown below, under some conditions, the photogenerated electron-hole pair remains bound; we refer to this neutral composite species as an exciton (58–60). Excitons can possess various characteristics—the electron and hole wave functions may strongly overlap or be offset from one another, as in a so-called charge-transfer state. Excitons can be stable over femtosecond to millisecond timescales, depending on the degree of attraction between the electron and hole. In some cases, excitons persist until the system relaxes back to the ground state (geminate recombination). Under other conditions, an exciton dissociates into an uncorrelated electron and hole, known as free charges, or charge carriers, which can then themselves relax to the ground state through so-called nongeminate recombination, where each carrier recombines with a newfound partner of opposite charge, or through nonradiative pathways. Exciton dissociation is mediated by temporal or spatial fluctuations or perturbations to the electron and hole wave functions that overcome their binding energy on timescales shorter than it takes for the system to return to its ground state. Both excitons and independent charge carriers can travel within the volume of a semiconductor over their lifetimes—a process especially important in optoelectronic energy transduction (e.g., photovoltaic or display technology), not only driven via electrical bias for charge injection or recombination but also when free of external driving forces. How does electronic energy transport occur upon photoexcitation, and what physical properties create the diversity of ways in which it occurs?

Multiple physical properties influence energy transport in semiconductors. Below, we organize these properties according to (a) their response to superposed electric fields, (b) the relative sizes of electronic and other interaction energies, (c) the different types of electronic interactions that mediate transport, and (d) the spatially dependent structural and energetic landscapes that emerge in semiconductors.

2.1.1. Screening and exciton binding energy. The dielectric constant, that is, the degree to which bound electrons can be polarized by an electric field, affects the nature of photoexcitations

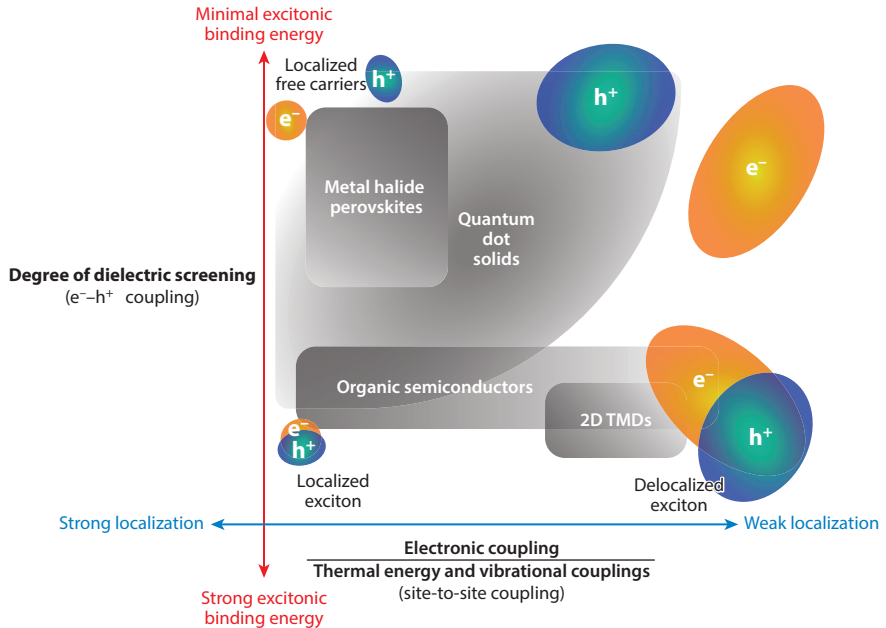


Figure 1

The various properties of photoexcited species in semiconductors and the multiple scales of energy transport. The degree of dielectric screening of the electron-hole attraction dictates the exciton binding energy (scaling as the inverse square of dielectric constant). Localization of wave functions is determined by the relative strength of electronic coupling to the coupling strengths between the energy carriers and lattice vibrations and thermal fluctuations. Together, these two properties determine to what extent electrons and holes are metastably bound and the extent of their delocalization. Abbreviation: TMD, transition metal dichalcogenide.

in semiconductors because it determines how effectively these electrons can screen the fields of photogenerated species (55, 57) (**Figure 1**). In semiconductors with smaller dielectric constants, the weakly screened electron-hole attraction is sufficiently strong that their locations and motions are correlated. In other words, the electron-hole binding energy (~ 0.5 eV) is high enough relative to the thermal energy (26 meV at room temperature) that the exciton is stable for an appreciable fraction of the excited system lifetime. This is typically the case in semiconductors made by packing small or polymeric π -conjugated organic molecules into a solid. By contrast, in high-dielectric-constant materials such as most inorganic semiconductors and in hybrid organic-inorganic metal halide perovskites, the electron-hole interaction is sufficiently screened that the photoinduced charge carriers scarcely interact with one another, and their transport is uncorrelated. An increasingly important exception to this trend is found in 2D semiconductors. Although in bulk (3D) transition metal dichalcogenides (TMDs), the high dielectric constant strongly screens electron-hole interactions, exfoliated 2D monolayers exhibit strong exciton binding energies comparable to those of organic semiconductors due to strong Coulombic attraction through the surrounding medium above and below the material plane.

TMD: transition metal dichalcogenide

2.1.2. Relative importance of electronic coupling. The strength of electronic coupling between the basic building blocks of the material, relative to its other energy scales (**Figure 1**), has important effects on the nature of photoexcitations in semiconductors. Electronic coupling is the

SELF-TRAPPING AND POLARONS

Polarons are important in many aspects of condensed matter physics that extend far beyond the topic of this review (169). Polaron is the so-called quasiparticle name given to a charge excitation in an ionic or polarizable solid material combined with the stabilizing deformation it induces in its surrounding lattice. It carries this deformation with it as it migrates, despite the additional associated drag. The electron-phonon coupling, that is, the lattice's propensity to deform combined with the degree of Coulomb attraction and repulsion with different ions or polarizable species in the lattice, is responsible for the stabilizing, or so-called self-trapping, deformations. One might draw a loose analogy between this self-trapping and a favorable solvation of a charged solute in a polar or ionic solution, except that the strain induced by distortions in a bonded lattice cannot relax in the way that a liquid can. In addition to charge carriers, excitons form weaker polarons that still affect excited-state dynamics in organic materials (170). The spatial extent of polaronic distortions depends on the electron-phonon coupling. Whereas small polarons, which are known to limit carrier mobility in organic semiconductors, are confined within a unit cell and exhibit incoherent hopping, large polarons extend over larger scales and exhibit band-like transport. The existence of large polarons in metal halide perovskites is a burgeoning area of research because these polarons emerge from a unique combination of the ionic lattice, strong polarizability, and moderate deformability (171, 172).

blanket term used to describe the electronic interaction between nearby sites in a semiconductor, which determines both the electronic structure and the mechanism for electronic excitations to move from place to place within the semiconductor; the various types of electronic coupling are described in detail below (55, 61). When this coupling is strong, the wave functions of excited state species, both charges and excitons, can be delocalized over scales much larger than individual structural components. At the other extreme, if carrier interactions with the surrounding crystal lattice, or more disordered matrix, or its vibrations (phonons) are comparatively strong, these interactions tend to localize the wave functions (see the sidebar titled Self-Trapping and Polarons). We distinguish the degree of delocalization of excitons with additional terminology: When the exciton wave function essentially extends throughout the material, we refer to it as a Wannier-Mott exciton, which has a low binding energy. When a lower dielectric constant and concomitant higher exciton binding energy in organic semiconductors localize an exciton, we refer to it as a Frenkel exciton.

2.1.3. Multiple microscopic mechanisms for energy transport. Next, we describe the various electronic coupling mechanisms that enable photogenerated energy carriers to move by an individual increment and how these individual steps cascade to yield long-range energy transport. Energy carrier migration is most simply characterized along a spectrum whose opposite extremes are wave-like and incoherent. [More sophisticated treatments explicitly incorporate effects of structural fluctuations on time scales similar to those of an individual step (62–65).] In wave-like transport, also referred to as band-like or ballistic, an energy carrier translates in a series of individually coherent segments. Most of its time is spent in motion, although the transport is segmented by instantaneous scattering with defects, phonons, or other carriers. In inorganic semiconductors, the distances between scattering events far exceed a bond length. In contrast, an incoherent transport increment constitutes a virtually instantaneous hop between two comparatively close sites (66). The residence time of an energy carrier at a site is much longer and is governed by a probability distribution. The timescale for an incoherent charge carrier hop in most materials we focus on in this review depends on how long a charge must wait before thermal fluctuations fleetingly bring its energy into resonance with the energy at its destination, as

prescribed by Marcus theory (67). Incoherent hops of Frenkel excitons typically occur between one chromophore (a light-absorbing unit the size of an excitonic wave function) and the next. Incoherent hopping of excitons often occurs through Förster resonance energy transfer (FRET) (68), the coupling of two chromophores' transition dipole moments. The Förster hopping rate is given by

$$k_{\text{Förster}} = \frac{1}{\tau} \left(\frac{R_0}{R} \right)^6, \quad 1.$$

where τ is the donor chromophore fluorescence lifetime; R is the distance between chromophores; and R_0 is the separation at which the energy transfer has 50% of its maximum possible efficiency. R_0 consists of many factors, including σ , a measure of resonance between the donor site emission and acceptor site absorption transitions (spectral overlap), even though the transfer process involves no emission or reabsorption. The probability of a Förster hop scales as $1/R^6$, limiting the practical hopping distance to 1–10 nm. At shorter chromophore separations, excitons hop via Dexter energy transfer (69), the coordinated exchange of one valence for one conduction electron between the two participating sites, that is, a tunneling effect that requires wave function overlap. Its rate therefore scales exponentially with R ,

$$k_{\text{Dexter}} \sim J\sigma e^{-R}, \quad 2.$$

with prefactors that include both spectral (σ) and orbital (J) overlap. Excitonic Dexter transfer is categorized as incoherent hopping because tunneling only occurs during rare instances when thermal fluctuations create the required resonance and overlap, similar to incoherent charge carrier hopping. Whereas singlet Frenkel excitons travel through both Förster and Dexter mechanisms, triplet excitons, which interact extremely weakly with light, predominantly employ Dexter transfer and travel far more slowly. Finally, the character of energy transport can be intermediate between wave-like and incoherent (70–74) and can also alternate between the two, with wave-like transit interleaved by slower incoherent hopping when a semiconductor comprises interspersed structurally ordered and disordered domains (75).

2.1.4. The spatioenergetic landscape. We consider multiple examples of how the extent of both dynamic and static perturbations to the degree of structural order in a semiconductor can strongly impact energy transport. Local spatial variations in structure translate into local variations in the energies and wave functions of excitons and charge carriers. Along with dynamic factors such as vibrations and thermal fluctuations, these produce a nonuniform energy landscape that biases their largely entropically driven translation from one location to another. We also show how low points in a material's energy landscape created by structural anomalies, impurities, or interfaces (grain boundaries or surfaces) can trap energy carriers, generating potentially tortuous transport.

2.2. Spatiotemporally Measuring Energy Flow

Multiple time-resolved microscopy-based approaches exist to spatiotemporally characterize energy flow. These all employ a local ultrafast (femto- to picosecond) laser pulse photoexcitation and subsequently image the spatial spreading of energy carriers (**Figure 2**) with fast time-resolution (femto- to nanoseconds). To do so, the photoexcitation/imaging sequence is repeated at each of multiple time delays until signal averaging produces a desired signal-to-noise ratio. The spot size

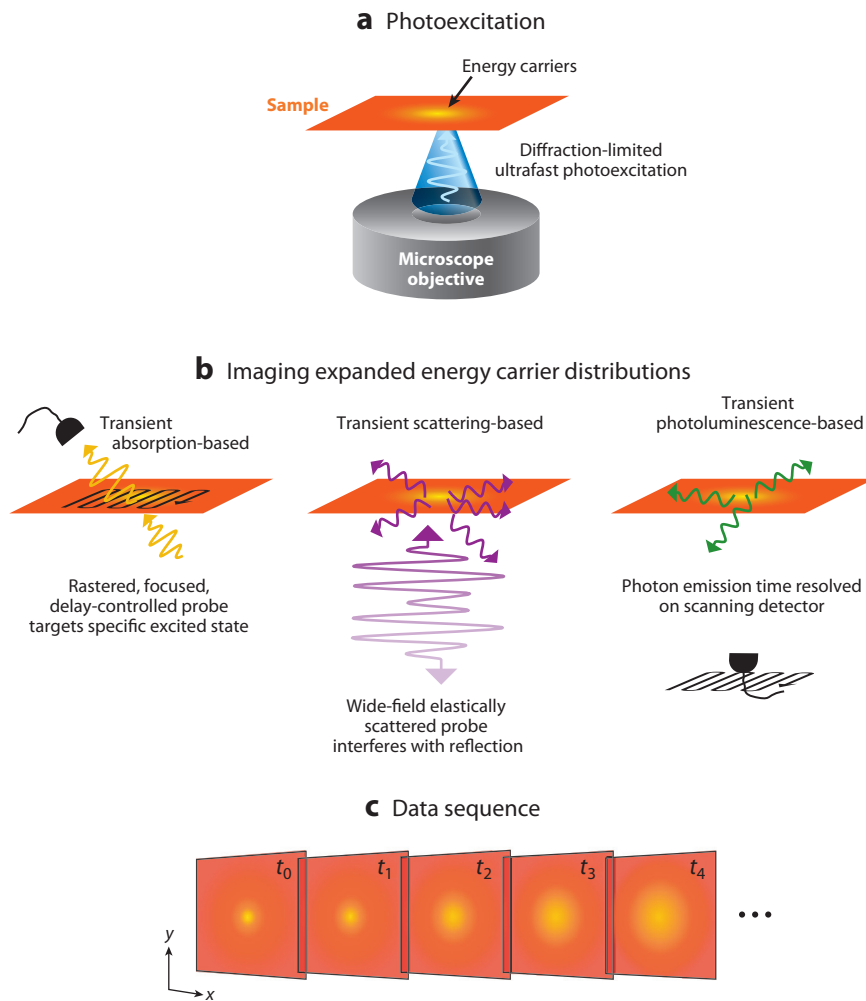


Figure 2

Similarities and differences among the three main approaches to spatiotemporally resolve energy migration. (a) Each is initiated by illuminating a small region of a semiconductor sample with an ultrashort, focused laser pulse to photogenerate energy carriers. (b) Each also produces a data sequence of spatial maps of the photoexcitation distribution expansion at a series of time delays. (c) The three approaches differ in the manner in which an individual image is collected: transient absorption approaches image with a rastering, coherent ultrafast probe light pulse; the time-resolved photoluminescence approaches described here measure arrival times of spontaneous emission at a rastering detector; and transient scattering approaches measure interference of elastically scattered light with a reflected reference beam in wide field. Note that microscope components such as the objective lenses, mirrors, and filters are not shown for each of the approaches to emphasize conceptual clarity.

of the photoexciting light pulse is generally limited to some fraction of the wavelength of visible light (hundreds of nanometers), but importantly, one can resolve changes in the spatial distribution of energy carriers (down to a few nanometers) from one time point to another. We distinguish three different types of detected signals, or forms of imaging contrast, that report the evolving footprint of transiting photoexcitations (**Figure 2**).

2.2.1. Transient absorption. Approaches based on TA directly measure the spatiotemporal population distribution of photoexcited species in a given state. A probe laser pulse resonant with a particular transition is rastered over a region of interest (ROI) centered on the excitation spot, which is created by a focused pump laser pulse (38, 42, 76). At each of a series of different pump-probe time delays, variations in the transmitted probe intensity due to minute amounts of stimulated emission or increased or decreased absorption, relative to the transmitted intensity obtained without first photoexciting the initial spot in the sample, are detected on a photomultiplier and correlated to the probe position on the sample. TA microscopy has the advantage of independently revealing the evolution of different excited state species, as long as the probe pulse wavelength resonantly addresses only one species' transition at a time, even if the sample does not luminesce. One challenge of TA microscopy is that the signal is orders of magnitude weaker than the intensity of the probe pulse (and its intensity fluctuations) that is detected along with it. Therefore, changes in the energy carrier distribution width typically reported thus far are resolved no better than ~ 50 -nm precision. Another challenge is that, for many samples, a moderately high photoexcitation fluence is required, which can precipitate nonlinear effects such as exciton-exciton annihilation that need to be accounted for in a model, but TA microscopy is capable of time resolution as fine as the pulse durations used (tens to a few hundred femtoseconds), typically scanned over a range of a few nanoseconds.

2.2.2. Transient photoluminescence. Another class of approaches measures the spatiotemporal distribution of photoexcitations via spatially resolved TRPL (35, 41). Rather than rastering a probe pulse, an avalanche photodiode is rastered in a highly magnified ($500\times$) image plane to collect a PL map over an ROI that contains the initial photoexcited spot (35). The luminescence that is detected is due to radiative recombination as excitations decay and return the system to the ground state, and images can be acquired at different times after photoexcitation, at different lateral positions, and in different spectral ranges. Correlating spectral information with the measured excited state lifetime, or radiative recombination rate, provides valuable detail on the kinetics of excitation population redistribution from the initially populated state into others at different energies. As in non-spatially-resolved TRPL, modeling can help to determine these kinetic parameters. TRPL-based microscopy is compatible only with luminescent materials. Yet, because it relies on detecting spontaneous emission—a background-free signal, as compared with the TA signal measured along with a probe laser pulse—it has the highest sensitivity and requires the lowest excitation fluences. Thus, TRPL-based microscopy can eliminate nonlinear effects and reduce the number of parameters in a model. That said, we note that TRPL microscopy results are more difficult to interpret in cases in which transport is dominated by free charge carriers—rather than excitons—because of the nonlinear dependence of the PL signal on the local density of electrons and holes.

2.2.3. Transient scattering. Approaches based on TS microscopy are largely intermediate between TA and TRPL microscopy. It measures spatiotemporal excitation distributions based on how photoexcited species alter the local dielectric constant (or index of refraction) of the material through elastic scattering of light (36). Because TS requires neither strongly absorbing nor strongly emissive samples, it is applicable to a wide range of materials and energy carriers (e.g., excitons, charge carriers, phonons), although it is not species-selective. Here, a time-delayed, wide-field probe light pulse, typically spectrally displaced from band edge transitions, illuminates an ROI that encompasses the local photoexcited spot, and the interference of probe light that scatters off of the locations containing energy carriers with probe light reflected off of the sample-substrate interface is captured on a camera image plane. The probe scheme, in

the absence of the initial photoexcitation, is known as interferometric scattering microscopy (77, 78), which is generally used to very sensitively observe sparse distributions of more slowly moving molecules or particles (79, 80). Here, it enables in situ correlation of energy flow with sample morphology provided by light scattering off of the sample microstructure. As with TA, TS images are obtained differentially, that is, by subtracting an interferometric scattering image of the sample without the pump excitation from the scattered image of the pumped sample. In its original diode laser implementation, TS time resolution is limited to ~ 100 ps, but it can cover an arbitrarily long range of time delays. The time resolution is, however, limited only by the laser pulse durations, down to approximately 50 fs. This lower bound is required to maintain an appropriate coherence length for its interferometric aspect. Because all pixels of an image are acquired on the camera simultaneously without any rastering, this approach is quite fast and has few-nanometer measurement precision. Its interferometric, phase-sensitive nature (81) also enables detecting out-of-plane transport.

The light source durations, time delay ranges, and detection schemes in each of the above microscopies are in principle interchangeable, and we hope that this review might encourage such exploration. For example, the different spatially resolved detection schemes, probe rastering in TA versus detector rastering in TRPL versus wide-field detection in TS, could be interchanged. We also note that, through the use of scanning probe microscopies, each of these modalities could be performed with enhanced spatial resolution, and concomitant enhanced complexity, although these approaches are beyond the scope of this review (82–85). Before reviewing applications from the existing literature, we first describe how data are analyzed and interpreted.

2.3. Extracting Microscopic Meaning from Spatiotemporal Data

In this section, we present the mathematical relationships between experimentally measured quantities and the underlying microscopic processes that contribute to their measured values. We pay particular attention to two limiting cases of microscopic transport processes—band-like transport and incoherent hopping—and to the many assumptions commonly made during the analysis of spatiotemporal transport data.

2.3.1. Diffusivity and diffusion length. Here, we show how the two distinct mechanisms for individual energy transport increments reviewed in Section 2.1, band-like (or coherent) and incoherent hopping, relate to quantities measured via a long sequence of increments, typically represented by a random walk and appearing diffusive at sufficiently macroscopic length scales.

Recall that band-like transport (**Figure 3a**) is characterized by coherent ballistic motion of a delocalized energy carrier that is frequently interrupted by scattering events that change the carrier's kinetic energy and momentum. This microscopic picture describes charge carrier diffusion in bulk inorganic semiconductors like silicon (86) and may describe the movement of excitons within coherently coupled aggregates of organic chromophores (65, 87, 88). The diffusivity ($\text{cm}^2 \text{s}^{-1}$) can be defined in terms of the carrier's average velocity, \bar{v} , and mean free path, λ_p , between collisions,

$$D = \frac{1}{3} \bar{v} \lambda_p. \quad 3.$$

The factor of one-third arises from the definition of the diffusivity along one spatial dimension, whereas the mean free path and average velocity are defined in three dimensions (i.e., $\bar{v} = \sqrt{v_x^2 + v_y^2 + v_z^2}$). If the carrier has a lifetime τ , then its diffusion length,

$$L_D = \sqrt{2D\tau} = \sqrt{\frac{2}{3} \bar{v} \lambda_p \tau}, \quad 4.$$

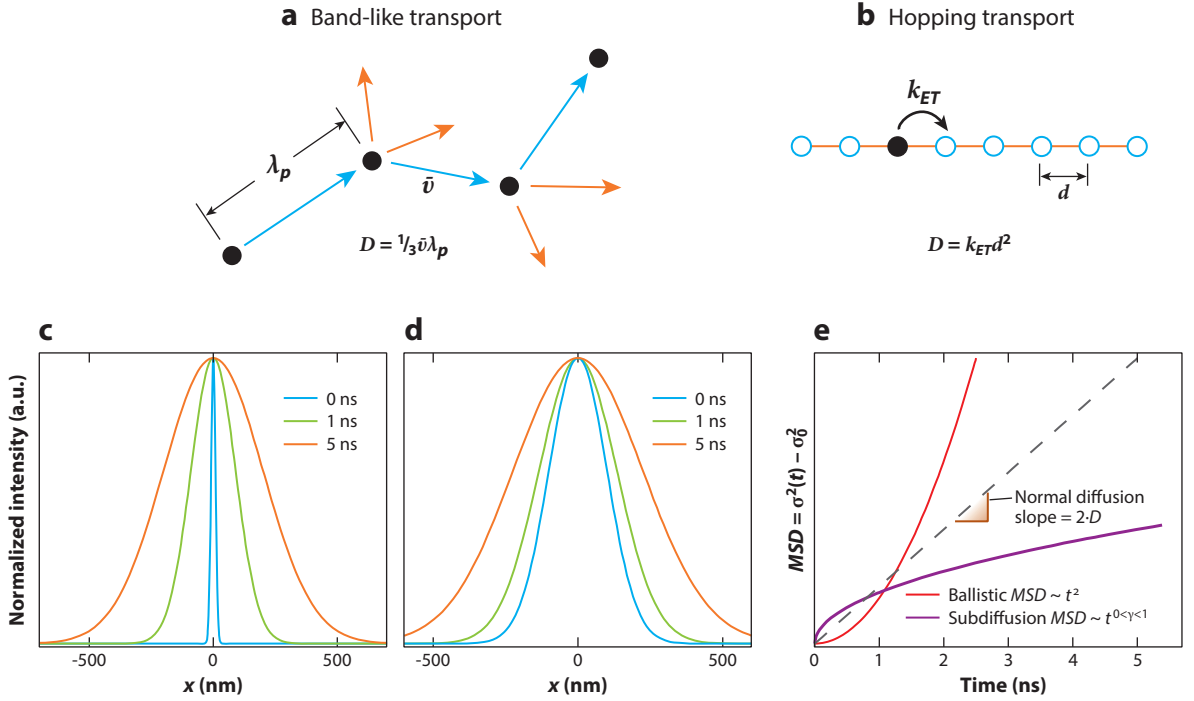


Figure 3

Diffusivity and quantitative analysis of spatiotemporal data. (a) Band-like transport processes. (b) Incoherent hopping transport processes. (c) Simulated diffusive broadening of a δ -function spatial distribution ($D = 0.04 \text{ cm}^2 \text{ s}^{-1}$). (d) Simulated broadening of a finite-sized distribution photoexcited by a focused Gaussian beam with $\text{FWHM} = 250 \text{ nm}$. (e) By plotting spatially resolved data as the change in the variance of the distribution, finite size effects are removed from the analysis and deviations from normal diffusive behavior can be revealed. Abbreviations: FWHM, full width at half maximum; MSD, mean squared displacement.

determines the characteristic root mean squared displacement of the energy carrier from its initial position at the end of its lifetime.

Separately, we saw that in incoherent hopping transport (**Figure 3b**), energy carriers spend most of their time localized on individual sites but make occasional instantaneous transitions via FRET or Dexter transfer to neighboring sites. For a simple cubic lattice of sites, the diffusivity in any direction is given by

$$D = k_{\text{ET}} d^2, \quad 5.$$

where k_{ET} is the transition probability per unit time (s^{-1}) to a neighboring lattice site (per pair of sites) and d is the center-to-center distance between lattice sites. The corresponding diffusion length is then

$$L_{\text{hopping}} = \sqrt{2k_{\text{ET}} d^2 \tau}. \quad 6.$$

For the case of charge carrier diffusion in semiconductors, the carrier diffusivity can be related to the carrier mobility, μ ($\text{cm}^2 \text{ V}^{-1} \text{ s}^{-1}$), through the Einstein relation,

$$D = \frac{\mu k_{\text{B}} T}{q}, \quad 7.$$

where k_b is Boltzmann's constant, T is the absolute temperature, and q is the elemental charge. For context, a charge carrier mobility of $\mu = 10 \text{ cm}^2 \text{ V}^{-1} \text{ s}^{-1}$ corresponds to a room temperature diffusivity of $D = 0.2 \text{ cm}^2 \text{ s}^{-1}$. In high-quality silicon crystals, the charge carrier diffusivity can be as high as $30 \text{ cm}^2 \text{ s}^{-1}$ with charge carrier lifetimes as long as 1 ms, resulting in diffusion lengths approaching 1 mm (86). By contrast, in organic molecular semiconductors, the singlet exciton diffusion length is typically $<10 \text{ nm}$ due to a $<10\text{-ns}$ exciton lifetime and $<10^{-4} \text{ cm}^2 \text{ s}^{-1}$ diffusivity (20). Consequently, spatiotemporal characterization of electronic energy transport in semiconductors requires experimental techniques with dynamic range spanning orders of magnitude in length and timescales.

2.3.2. What is actually measured? Spatiotemporal measurements of electronic energy migration—whose beginnings are rooted in transient grating experiments (9, 89) and coupling a streak camera to a microscope (90)—inherently measure the rate of energy transport (i.e., the diffusivity of the photoexcited carrier population). This is in contrast to steady-state patterned illumination for far-diffusing species (91–93) or more conventional approaches, such as interfacial quenching (18–26), which primarily report the spatial extent of migration over the course of the carrier lifetime (i.e., the diffusion length). While these quantities can be easily interrelated for normal diffusion processes, the advantage of a spatiotemporal approach is its ability to identify and characterize transport behavior that deviates from normal diffusion.

For a normal diffusive transport process, the probability density distribution n along any dimension x is given by

$$\frac{\partial n(x, t)}{\partial t} = D \frac{\partial^2 n(x, t)}{\partial x^2} - \frac{n(x, t)}{\tau}, \quad 8.$$

where D is the diffusivity in the x -direction and τ is the natural decay lifetime of the species. If the initial distribution of energy carriers at $t = 0$ were a δ function at $x = x_0$, then the distribution at any later time t would be a Gaussian function with monotonically increasing width in time (**Figure 3c**),

$$n(x, t)|_{\delta(t=0)} = G(x, t) = \exp(-t/\tau) \frac{1}{\sqrt{4\pi Dt}} \exp\left[-\frac{(x - x_0)^2}{4Dt}\right]. \quad 9.$$

In reality, the initially excited distribution $n(x, 0)$ is determined by the laser intensity profile focused on the sample. In this case, the probability distribution at any time t is a convolution of the initial distribution with the time-dependent Gaussian function derived above (**Figure 3d**),

$$n(x, t) = n(x, 0) * G(x, t) = \exp(-t/\tau) \frac{1}{\sqrt{4\pi Dt}} \int_{-\infty}^{+\infty} n(x, 0) \exp\left[-\frac{(x - x_0)^2}{4Dt}\right] dx. \quad 10.$$

Typically, we normalize the signal intensity profile at each time t to neglect the exponential decay term and more easily identify the spatial broadening of the distribution. Assuming instantaneous photoexcitation by a focused Gaussian beam, the variance (square of the standard deviation) of the spatial distribution at any time t is

$$\sigma^2(t) = \sigma_0^2 + 2Dt, \quad 11.$$

where σ_0^2 is the measured variance of the distribution at $t = 0$. The corresponding mean squared displacement (MSD) due to transport is given by

$$MSD = \langle x(t)^2 \rangle - \langle x(0)^2 \rangle = \sigma^2(t) - \sigma_0^2 = 2Dt. \quad 12.$$

Importantly, Equation 12 indicates that the initial size of the distribution does not matter as long as we can accurately resolve the temporal change in width of the distribution with sufficient precision (**Figure 3e**). The data manipulation in Equation 12 also eliminates effects of finite detector size, point spread function of the collection system, and non-Gaussian excitation profile, although these effects still impact the signal-to-noise ratio (34).

It is important to emphasize that direct comparison of Equations 11 and 12 to experimental data is appropriate only if the measured signal (for example, absorbance) is linearly proportional to the local density of the diffusing species (for example, the exciton population). If there are second- or third-order decay terms in Equation 8, then the signal intensity profile at each time t should not be normalized. Notable examples include exciton-exciton or exciton-polaron annihilation and the use of TRPL microscopy to visualize transport in materials in which excitons readily dissociate into free charge carriers. In these cases, the spatial width of the signal will broaden faster than predicted by Equations 11 and 12 due to density-dependent recombination, which is spatially nonuniform.

There is occasionally confusion among practitioners regarding the choice of the numerical constant (2, 4, or 6) in Equation 12 or in the calculation of the diffusion length, depending on whether transport proceeds in one, two, or three dimensions. This numerical constant depends only on how the variance of the spatial distribution is calculated and not on the sample dimensionality or how the data were collected. A factor of 4 is appropriate if the variance is calculated by integrating 2D displacement data in radial coordinates; a factor of 6 is appropriate if the variance is calculated by integrating 3D displacement data in spherical coordinates. In most cases, even when multidimensional data are collected, MSD data are plotted along a single Cartesian direction (**Figure 3c–e**) so that a factor of 2 is appropriate.

In all cases, a diffusion length is properly defined as the projection of the total 3D displacement of the exciton or charge carrier onto a single axis, $L_D = \sqrt{2D\tau}$, where τ is the carrier lifetime. The factor of 2, however, is often dropped, resulting in a standard definition, $L_D = \sqrt{D\tau}$.

Because the measurement techniques presented here are based on resolving absolute changes in the spatial emission/absorption/scattering profile over time, there is in principle no fundamental limit to the minimum diffusion length that can be resolved. In practice, aberrations in the optical system, mechanical drift over the course of the experiment, and sensitivity to the choice of fitting function make it difficult to resolve migration lengths shorter than ~ 10 nm. Additionally, the signal-to-noise ratio is limited by the natural lifetime of the chromophore under investigation; materials with slower natural decay rates necessitate longer waiting times between photoexcitation events, limiting the number of acquisitions per second.

2.3.3. Nondiffusive transport phenomena. When looked at rigorously, diffusivity is an equilibrium concept, yet energy carriers excited by short-duration laser pulses are often out of equilibrium during a spatiotemporal measurement. Indeed, the advantage of such techniques is their ability to identify and characterize transport behavior that deviates from normal diffusion. Equation 12 constitutes a general starting point for the analysis of such nondiffusive transport phenomena as well.

In contrast to diffusive transport, where the average displacement increases as the square root of time, $\Delta x \sim t^{1/2}$ or $MSD \sim t$, ballistic transport is characterized by a displacement increasing linearly with time, $\Delta x \sim t$ or $MSD \sim t^2$. Transport processes in which the mean-squared-displacement grows sublinearly, $\Delta x \sim t^{0 < \gamma < 0.5}$ or $MSD \sim t^{0 < \gamma < 1}$, are often characterized as subdiffusive transport processes (**Figure 3e**), though they are more accurately described as nonequilibrium transport processes. Many emerging semiconductors, including molecular crystalline semiconductors, semiconducting polymers, and colloidal QD arrays, feature a significant amount of site-to-site

energy disorder. In such systems, the growth of the MSD is observed to slow down over time as energy carriers migrate energetically downhill and subsequent hopping events become less likely. In such cases, it is the probability density function describing the energetic distribution of charge carriers or excitons that changes in time, rather than the intrinsic diffusivity of the material system. Formally, the diffusivity is a time-independent function of the occupied density of states; as charge carriers relax to form a thermalized Boltzmann distribution over the disordered site energy landscape, the constant, equilibrium diffusivity is ultimately reached. In contrast, true subdiffusive processes continue to slow down indefinitely.

3. APPLICATIONS OF SPATIOTEMPORAL CHARACTERIZATION OF ELECTRONIC ENERGY TRANSPORT

In this section, we review examples in the literature in which spatiotemporal measurement techniques were used to investigate electronic energy transport in emerging semiconductor materials. We begin with QD solids in Section 3.1, progress to the broad field of organic semiconductors in Section 3.2, discuss recent work in the rapidly growing field of organic-inorganic metal halide perovskites in Section 3.3, and close with 2D TMDs in Section 3.4. The list of experiments presented is not exhaustive, unfortunately omitting, for instance, an emerging emphasis on transport phenomena at heterostructure interfaces (94–97).

3.1. Exciton Transport in Colloidal Quantum Dot Solids

Colloidal QDs are semiconductor nanocrystals whose optical and electronic properties are derived in part from quantum confinement of charge carriers (31). QDs possess discrete electronic energy levels near the band edge—rather than the delocalized continuous energy bands typical of bulk inorganic semiconductors—that more closely resemble the excited states of atoms and molecules than crystalline solids. The semiconductor core is typically ~ 2 – 10 nm in diameter and may be coated with an epitaxial shell that electronically isolates the excited state within the core of the nanocrystal (98) (Figure 4a). Prepared as colloidal suspensions, QDs typically include a layer of surface-bound organic molecules. Prototypical systems include visible-emitting CdSe QDs and

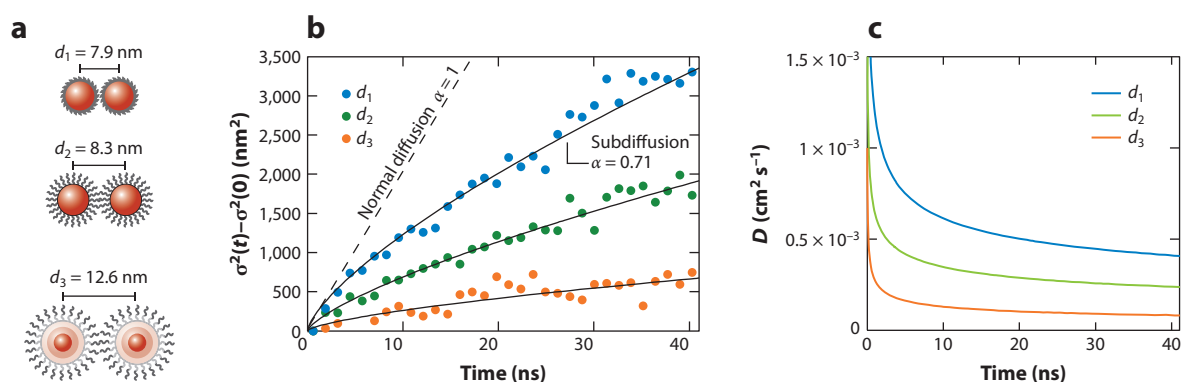


Figure 4

Nonequilibrium exciton transport in quantum dot (QD) solids. (a) Schematics of three different batches of CdSe/CdZnS core/shell QDs coated with surface ligands of different lengths and CdZnS shells of different thicknesses. (b) Corresponding mean squared displacement (MSD) versus time plots for the three samples, measured by time-resolved photoluminescence microscopy. The MSD grows sublinearly in time for all three samples. (c) Diffusivity of the exciton population versus time for each sample, extracted from the MSD versus time plots shown in panel b. Figure adapted from Reference 34 with permission; copyright 2014 American Chemical Society.

near-infrared-emitting PbS QDs, although there is increasing interest in lead halide perovskite QDs (99), such as CsPbBr₃, and heavy-metal-free compounds, such as InP.

Brightly emissive QDs have already been commercialized for use as luminescent down-converters in televisions and mobile device displays (100). However, their use in solar cells (101) and light-emitting devices (102) has lagged behind, in part because of a lack of control over charge and exciton transport in QD solids. Through colloidal self-assembly, beautifully ordered QD superlattices can be prepared that inspire visions of designer solids with precisely tuned functionality through the use of QDs as atom-like building blocks (103, 104).

3.1.1. Nonequilibrium transport in quantum dot arrays. Despite some controversy regarding the nature of charge transport in QD solids (98, 105), physical understanding of exciton transport in visible-emitting CdSe QD solids is firmly established (34, 106, 107). Despite surface-to-surface separation distances that are much shorter than the diameter of the semiconductor core, exciton transport in CdSe QD solids is well described by weak coupling of point dipoles located at the center of neighboring QDs, and the corresponding exciton hopping rates can be predicted by FRET. Consequently, exciton transport in CdSe QD solids can be thought of as a classical random walk wherein excitons undergo discrete hops from nanocrystal to nanocrystal.

Because of their bright and stable luminescence and well-behaved decay dynamics, CdSe QDs were one of the first material systems whose exciton transport behavior was investigated using TRPL microscopy. Tisdale and coworkers (34) measured the transient spatial broadening of thin-film PL for three different QD films (**Figure 4b**). As expected, the MSD grew more slowly when neighboring QDs were spatially separated by longer surface ligands or thicker shells. Surprisingly, however, in all three samples the MSD grew sublinearly, revealing a decreasing diffusivity of the exciton population over time (**Figure 4c**). Using spectrally resolved TRPL in conjunction with kinetic Monte Carlo simulations, Tisdale, Willard, and coworkers (34, 108) showed that this behavior arises from energetic disorder within the QD solid. While these observations were initially characterized as subdiffusive transport, the behavior observed is more accurately described as nonequilibrium transport (109) (Section 2.3).

3.1.2. Beyond Förster hopping? An interesting remaining question is whether exciton transport in QD arrays can ever deviate from the simple FRET hopping picture. Weiss, Schatz, and coworkers (110) noted the breakdown of the point dipole approximation in PbS QD solids linked by mercaptoalkanoic acids when the inter-QD separation distance was less than a critical value. Huang and coworkers (47) measured an exciton diffusivity of 0.02 cm² s⁻¹ in highly ordered and energetically homogeneous CdSe QD superlattices using TA microscopy. The value is an order of magnitude larger than that observed in the disordered QD solids measured by Tisdale and coworkers (34), but still in agreement with Förster theory. More recently, Roberts and coworkers (111) extracted exciton hopping times of only ~200 fs in CdSe QDs capped with phenyldithiocarbamate ligands using spectrally resolved TA. Phenyldithiocarbamate ligands have previously been shown to form hybridized electronic states with the CdSe core, delocalizing the hole wave function outside the nanocrystal (112). It is difficult to reconcile such fast transport timescales within a Förster hopping picture, but these timescales could be explained by strong exchange coupling between neighboring QDs. QD arrays that are electronically coupled by inorganic linkers have achieved charge carrier mobilities of >10 cm² V⁻¹ s⁻¹, which corresponds to ~1-ps charge hopping times (6). There is no reason, in principle, why Dexter or other exchange-mediated exciton hopping processes (113) could not outpace Förster hopping in electronically coupled QD arrays. At low temperature, partially coherent exciton transport may even be possible (109), but this may be difficult to prove using only the spatially resolved techniques presented here.

3.2. Exciton Transport in Organic Semiconducting Solids

Semiconducting materials composed of organic small molecules or polymers have been studied for the past several decades (57, 114, 115) and lend themselves to potential applications in flexible electronics through energy-efficient solution processing. Through synthetic control, limitless variety and tunability of molecular building blocks enable substantial tunability in electronic properties (116, 117). They assemble into a solid through van der Waals interactions, a much weaker attraction than bonding in inorganic semiconductors (57, 114, 118). Organic semiconductors span a large dynamic range in structural order, from perfect single crystals of small molecules like polyacenes to amorphous or glassy tangles of high-molecular-weight π -conjugated polymers (plastics). Their electronic structure and dynamics can be quite heterogeneous because they are locally determined by particular intermolecular packing configurations through the coupling of molecular transition dipole moments (119–122) or, more generally, of electronic transition density (123) at different sites. Because of their low dielectric constants, Frenkel excitons are the typical photo-generated energy carriers in organic semiconductors (**Figure 1**), and exciton transport generally involves incoherent hops. Due to the large number of molecular degrees of freedom, excitons localize on few molecules or moieties unless a particularly rigid structure is formed that can sustain delocalization and wave-like transport.

3.2.1. Exciton transport in molecular crystals. The very first high-resolution spatiotemporally resolved measurements of energy transport were performed in organic semiconducting films. Bulović and coworkers (35) resolved the expansion of a localized population of excitons in tetracene films (**Figure 5a**) as a function of space, time, and exciton transition energy, using the TRPL-based approach. The photophysics of tetracene solids involves singlet fission into pairs of lower-energy, optically dark triplet excitations (124–129) (**Figure 5b**; also see the sidebar titled Singlet Fission), followed by some amount of the reverse process of triplet fusion, whereupon delayed fluorescence can be emitted from a regenerated singlet excitation on a microsecond timescale (130). Exciton migration occurs both before and after each of the fission and fusion processes, although the mechanism for transport of singlets is Förster-mediated and that for triplets relies on slower, shorter-range Dexter transfer. A kinetic model including singlet-triplet interconversion and diffusion was used to interpret the delayed fluorescence intensity distribution dynamics in both crystalline and polycrystalline films. It revealed that triplet migration contributes most to the population expansion in tetracene and also showed a diffusive-to-subdiffusive transition due to exciton trapping outcompeting excitation transfer as the average exciton energy decreased in time (**Figure 5c**). This transition, however, occurred earlier in the more disordered films (0.35 versus 2 μ s), establishing a clear correlation between film morphology, exciton trapping, and the exciton transport character.

This initial high-resolution study, partly facilitated by extremely long diffusion lengths ($L_D = 440$ nm) since triplet excitons scarcely couple to light, shows that exciton trapping at grain boundaries substantially limits transport. Microscopy based on TS recently resolved this impact of grain boundaries even more directly. Delor et al. (36) demonstrated that the expansion of an initial localized exciton distribution in polycrystalline 6,13-bis(triisopropylsilyl)ethynyl (TIPS) pentacene depends intimately on the proximity to interfaces between crystal grains. The spatiotemporal expansion of exciton populations initially freely diffusing in a crystalline region abruptly changed its rate upon approaching an interface (**Figure 5d**). The mean squared expansion versus time mimics the piecewise behavior seen in **Figure 5c** and additionally pinpoints where in the polycrystalline morphology it is observed.

TA-based experiments have also been performed to study spatiotemporal exciton dynamics in small-molecule organic semiconducting films that exhibit singlet fission. An ultrafast probe pulse

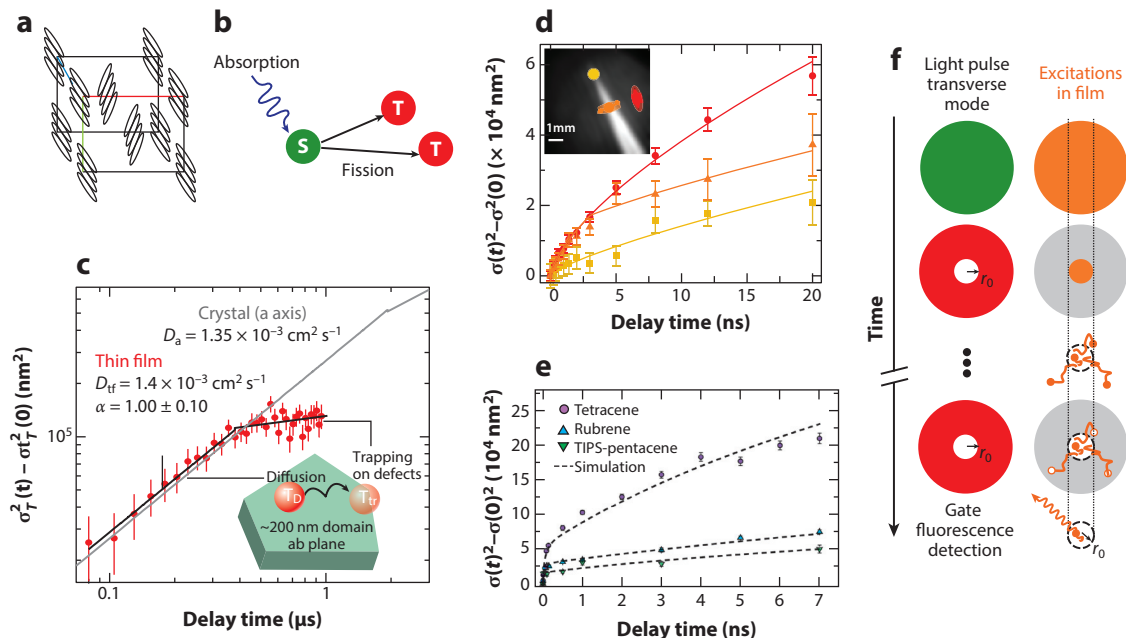


Figure 5

Exciton transport in organic semiconductors. (a) Example structure of tetracene molecular crystal. (b) Two triplet (T) excitons are created from a single photon absorption event due to singlet (S) fission. Mean squared expansion of exciton distributions in (c) tetracene and (d) 6,13-bis(triisopropylsilylethynyl) (TIPS)-pentacene polycrystalline films deviates from diffusive transport due to encounters with grain boundaries. The inset in panel d color-codes for the three different trajectories plotted by indicating the spot near (red), within (orange), or at the apex (yellow) of a wedge-shaped (white) crystalline domain. (e) Comparison of exciton population mean squared expansion in three different molecular crystals using transient absorption microscopy. (f) The TRUSTED (time-resolved ultrafast stimulated emission depletion) pulse scheme allows measurement of short exciton migration lengths in conjugated polymer solids. Panel c adapted from Reference 35 with permission. Panel d adapted from Reference 36 with permission. Panel e adapted from Reference 43 with permission. Panel f adapted from Reference 44 with permission.

SINGLET FISSION

Singlet fission could have an important impact in enhancing power conversion efficiencies of solar cells. Similar to multiexciton generation in nanocrystals, singlet fission involves the decomposition of a singlet exciton into two daughter triplet excitons, each with approximately the energy of the original singlet. Fissioning organic semiconductor films employed as sensitizing or active layers in solar cells offer the possibility to generate two quanta of energy (ideally, two electrons and two holes collected as a photocurrent) from absorption of a single photon (124). The reversibility of singlet fission can aid exciton transport by balancing faster singlet transfer with extended, dark triplet exciton lifetimes. Singlet fission is a rapidly growing research area not only because of its technological potential but also because its mechanism is challenging to describe theoretically and characterize directly with experiments (125–127, 173, 174). Approaches to elucidate the underpinnings of the phenomenon include engineering molecular crystals with controlled, variable packing motifs; generating isolated dimers of fissioning molecules that adopt controlled intermolecular configurations (175, 176); undertaking many ultrafast optical spectroscopy experiments (43, 128, 177–179); and developing substantial electronic structure calculation methodologies (129, 173, 174, 180). Near-perfect singlet fission efficiencies have been measured in some configurations, yet devices employing this enhancing approach have yet to be widely adopted.

that can be tuned to the distinct excited-state absorption transitions of singlet or triplet excitons enables selective probing of the instantaneous balance of their respective populations. In tetracene, TIPS-pentacene, and rubrene single crystals, Huang and coauthors (42, 43, 45) focused specifically on how interconversion between bright singlet and dark triplet excitons affects energy transport as a function of molecular packing and singlet fission energetics. For example, based on kinetic modeling, they conclude that tetracene crystals promote the longest exciton transport by combining moderate singlet and triplet diffusivities and a higher fission rate that generates the most substantial triplet population. Tetracene outperforms TIPS-pentacene, despite its higher singlet diffusivity, and rubrene, despite its higher triplet diffusivity. Although in each material, triplets travel three orders of magnitude more slowly than singlets ($\sim 10^{-3}$ versus ~ 1 $\text{cm}^2 \text{s}^{-1}$), TA microscopy shows how multiple parameters must balance to optimize energy diffusivity in crystalline organic semiconductors.

An additional asset of TA-based microscopy is that it can spatiotemporally follow earlier-time dynamics, when coherent effects are important. Huang and coworkers (45, 46) have studied exciton migration on few-picosecond timescales in individual tubular porphyrin-based aggregate nanotubes where exciton delocalization may extend over tens of to several hundred molecules. Here, intermolecular coupling and static disorder have similar, few-hundred-wavenumber-sized strengths. Although TA trades off the number of measured time delays in favor of spatial resolution, the data suggest few- $\text{cm}^2 \text{s}^{-1}$ diffusive transport systematically slightly exceeding the upper bound on incoherent hopping. Technical advances to balance such data collection with spatial sensitivity should enable increasingly rigorous tests of electronic energy flow models.

3.2.2. Exciton transport in amorphous conjugated polymer solids. The development of TRUSTED (time-resolved ultrafast stimulated emission depletion), a superresolution fluorescence-based approach, has enabled more direct characterization of exciton migration in more disordered conjugated-polymer-based semiconductors whose commensurately short, $\lesssim 20$ -nm exciton diffusion lengths have evaded the three main spatiotemporally resolved approaches discussed in this review (44). Sensitivity to detect short migration trajectories is achieved by defining excitation profiles with unusually sharp boundaries. Immediately following diffraction-limited preparation of an exciton population, Penwell et al. (37; see also 131) reduce it to a sub 100-nm-diameter population using an annular stimulated emission depletion light pulse (**Figure 5f**). The sharp circular population boundary obtained using nonlinear saturation of electronic quenching transitions as a function of patterned illumination intensity (37) [a strategy also explored by Grumstrup and coworkers (132, 133) with TA microscopy and King & Granick (134) with electroluminescence] drives radial diffusive expansion that is detected on pico- to nanosecond timescales using a second, time-delayed stimulated emission depletion pulse in combination with time-gated fluorescence detection (135). TRUSTED thus yielded $L_D = 16$ nm in amorphous poly[2,5-di(hexyloxy)cyanoterephthalylidene] with few-nanometer sensitivity. In combination with modeling, Penwell and coauthors (44) also discovered unexpectedly that exciton migration was diffusive despite substantial structural disorder, indicating that widely and rapidly fluctuating exciton transition energies at a given location can compensate for broad site-to-site energetic disorder to avoid the nonequilibrium behavior seen in QD solids.

3.3. Charge Carrier Transport in Organic-Inorganic Metal Halide Perovskites

While the previous two applications of spatiotemporal microscopy focused on exciton migration in low-dielectric semiconductors, we now turn to an example in which a higher dielectric constant yields charge carriers as the main species for photoinduced energy flow (**Figure 1**). To do so we

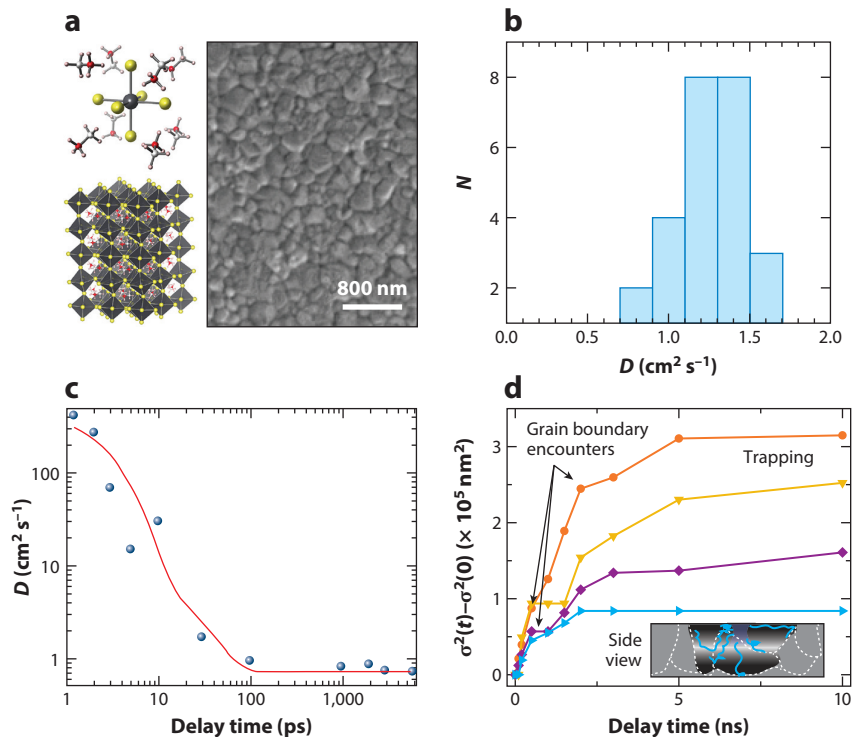


Figure 6

Spatiotemporal charge carrier migration resolved in MAPbI₃. (a) MAPbI₃ is pictured on multiple scales: at the scale of a single perovskite unit cell, a small volume of the perovskite crystal lattice, and a solution-cast polycrystalline film resolved in scanning electron microscopy. (b) Distribution of diffusivities obtained by measuring 25 different crystalline regions of interest with transient absorption (TA) microscopy. (c) Time-dependent effective diffusivity measured as hot carriers migrate, cool, and assume diffusive behavior with TA microscopy. (d) Mean squared expansion of charge carriers in different directions, all originating from the same spot, shows segmented dynamics, first alternating between free diffusion and hindered lateral motion before trapping sets in. (*Inset*) Side view of subsurface carrier trajectories upon grain boundary encounter. Panel a adapted from Reference 15 with permission; copyright 2015 American Chemical Society. Panel b adapted from Reference 50 with permission; copyright 2017 American Chemical Society. Panel c adapted from Reference 39 with permission from AAAS. Panel d adapted from Reference 36 with permission.

focus on hybrid organic-inorganic lead halide perovskite semiconductors, primarily methylammonium lead iodide (MAPbI₃) (Figure 6a), whose solution-processed solar cells' rapidly increasing power conversion efficiency has drawn much attention in recent years (136–139). Unfortunately, the many variations in perovskite material composition and processing and in the microscopies used to characterize them cannot all be included within the scope of this review (140, 141). Along with stability, a major challenge in developing these enigmatic materials into viable active layers in photovoltaic, light-emitting, and even lasing devices is the high variability in material properties—both across different films or preparations and among domains in a given polycrystalline film (15, 85, 142–146). Fundamental spatiotemporally resolved energy transport studies focusing on both the intrinsic semiconductor properties obtained within individual domains and the effect of polycrystalline film morphology on carrier transport are well suited to identify systematics to control the variability.

3.3.1. Intrinsic transport properties. Approaches based on TA employ various probe wavelength selection strategies to decouple spatiotemporal carrier distribution evolution from ultrafast processes seen in perovskite spectroscopy, such as band gap renormalization, band filling, and line broadening (147). Grumstrup and coworkers (50) determined the intrinsic carrier diffusivity within a total of 25 different crystalline domains of MAPbI₃. Their mean intradomain diffusivity of $\sim 1 \text{ cm}^2 \text{ s}^{-1}$ that is observed over a range of carrier densities up to $4 \times 10^{19} \text{ cm}^{-3}$ is attributed to substantial dielectric screening in and electron-phonon coupling to the ionic lattice and corroborates more traditional bulk measurements of large-area single-crystal samples. The statistical characterization performed also establishes the variability in diffusivity, with values ranging between ~ 0.7 and $1.7 \text{ cm}^2 \text{ s}^{-1}$ (**Figure 6b**). This same group has proceeded to investigate the physical origin of the measured diffusivities by combining TA-based measurements with ground- and excited-state reflectivity imaging (51). The two different types of imaging allow more unequivocal extraction of carrier scattering lifetime and effective mass.

3.3.2. Morphology affects transport. Beyond intrinsic properties, Huang and coworkers (48) have used TA microscopy on polycrystalline regions of MAPbI₃ films, for example, comparing TA maps of carrier migration in films with different grain sizes (52). They have also explored transport dynamics of carriers photoexcited well above the conduction band edge, suggesting quasiballistic expansion of distributions over several hundred nanometers within tens of picoseconds, prior to resumption of diffusive behavior (39) (**Figure 6c**). This effect could contribute to photovoltaic device efficiency.

TS-based dynamic imaging complements TA-based findings, demonstrating that a parameter like diffusivity in these highly heterogeneous materials does not fully capture the essential characteristics of carrier transport (36). Carriers locally alter a perovskite film's dielectric function and corresponding TS imaging contrast. Delor et al. (36) show how higher grain boundary densities decrease average carrier diffusivity 10- to 20-fold and that diffusive expansion of photogenerated carrier distributions is substantially slowed at grain boundaries. More specifically, grain boundaries impede the in-plane diffusion to which all spatiotemporal imaging approaches are sensitive, but TS interferometric phase sensitivity reveals that carriers are channeled deeper into a grain until encountering lower-resistance interfacial areas through which they can emerge into a neighboring grain (15, 148). This behavior produces terracing in the carrier distribution expansion versus time measured along different lateral directions (**Figure 6d**). Furthermore, the minimal slope of these curves beyond several nanoseconds of evolution suggests that carriers localize at traps on timescales an order of magnitude shorter than carrier lifetimes. The implication of this finding is that extrapolating carrier migration lengths from a combination of carrier lifetimes and their initial (after only nanoseconds) diffusivity in cases when diffusive behavior does not persist could lead to a significant overestimation of migration lengths.

3.4. Exciton Transport in Two-Dimensional Transition Metal Dichalcogenides

In 2010, Heinz and coworkers (149) isolated atomically thin flakes of MoS₂, a layered TMD composed of 2D sheets held together by weak van der Waals interactions. Similar to graphene, TMD crystals can be exfoliated down to single layers whose physical properties differ from the bulk crystal. Unlike graphene, however, most single-layer TMDs are direct gap semiconductors exhibiting strongly bound excitonic states with resonances spanning the near infrared to visible regions of the spectrum. Following this discovery, a wide variety of semiconductor devices has been

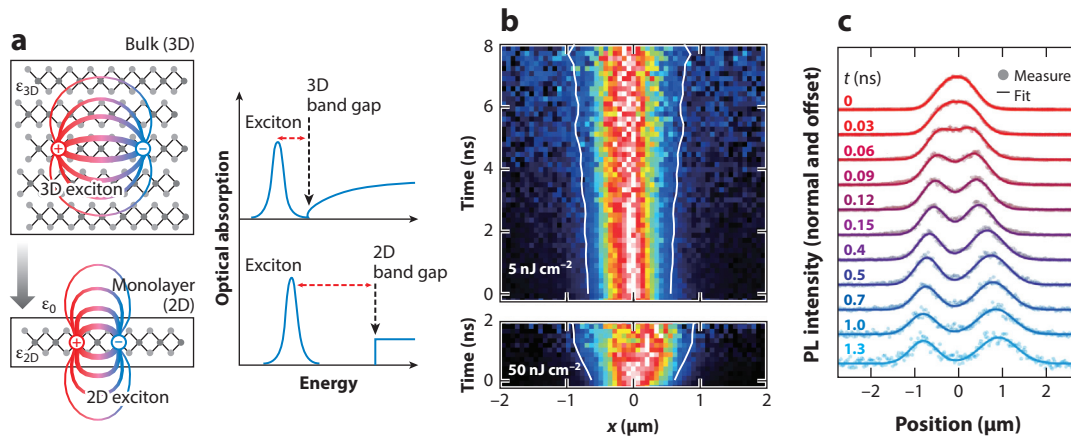


Figure 7

Exciton transport and annihilation in TMDs. (a) Dielectric confinement in monolayer TMDs leads to large exciton binding energies. (b) Exciton-exciton annihilation in areas of high photoexcitation density can cause the measured width of the spatial distribution to rapidly broaden if the excitation density is not carefully controlled. (c) High excitation densities can lead to halo effects in spatially resolved measurements, wherein the spatial distribution has apparent memory of its past excitation density. Abbreviations: PL, photoluminescence; TMDs, transition metal dichalcogenides. Panel *a* adapted from Reference 154 with permission; copyright 2014 American Physical Society. Panel *b* adapted with permission from Reference 53. Panel *c* adapted from Reference 41 with permission; copyright 2018 American Physical Society.

demonstrated, including field-effect transistors (150), light-emitting diodes (151), lasers (152), and polaritonic microcavities (153).

Bound excitonic states with in-plane oriented transition dipoles arise in part from strong dielectric confinement effects (154–156) (Figure 7a). Despite the generally large dielectric constant of a TMD monolayer, Coulombic interactions between electrons and holes are poorly screened out of plane. Resulting effects on electronic and excitonic properties include nonhydrogenic excitonic Rydberg series (154, 155), external-environment tuning of exciton and trion energies (157) and their multibody interactions (53), strong tunable interlayer coupling in TMD heterostructures (158), and prominent many-body effects (159), including strongly bound trions (156) and biexcitons (160).

3.4.1. Exciton diffusion and annihilation. Because monolayer TMDs simultaneously exhibit strongly bound excitonic states ($E_b \sim 320$ meV in monolayer WS_2) (154) and continuous conduction and valence bands, they represent an interesting intermediate case in which excitons exhibit both Wannier and Frenkel character. Huang and coworkers (40) recently used TA microscopy to spatially resolve exciton transport in WS_2 . They measured the exciton diffusivity in exfoliated WS_2 monolayers to be $2.0 \text{ cm}^2 \text{ s}^{-1}$, but only $0.1 \text{ cm}^2 \text{ s}^{-1}$ in CVD-grown monolayers. Additionally, they observed that the exciton diffusivity monotonically increased with increasing flake thickness. These two observations led them to conclude that exciton transport in TMD monolayers is suppressed by defect scattering. A similar conclusion was reached by Tisdale, Javey, and coworkers (53), who used TRPL microscopy to spatially resolve exciton transport in acid-treated monolayers of exfoliated MoS_2 . They measured exciton diffusivities as small as $0.06 \text{ cm}^2 \text{ s}^{-1}$, which they attributed to long residence times in spatially localized dark exciton states associated with sulfur site vacancies that are passivated by the superacid conjugate base anion (53, 161).

In both studies, accurate measurement of the exciton diffusivity was made difficult by strong exciton-exciton annihilation effects, which lead to nonradiative recombination in areas of high excitation density (40, 53) (**Figure 7b**). In acid-treated MoS₂, signatures of exciton annihilation were observed at excitation densities as low as <10 excitons μm⁻² (53, 162). Exciton-exciton annihilation is particularly problematic for spatially resolved transient spectroscopy experiments because the exciton density varies as a function of spatial position. Interestingly, Tisdale, Javey, and coworkers (53) found that annihilation could be dramatically suppressed by transferring TMD monolayers to substrates with a larger dielectric constant.

In a closely related study, Chernikov and coworkers (41) used a streak camera to perform TRPL microscopy investigations of exciton transport and annihilation in SiO₂-supported and freestanding WS₂ monolayers. At low fluence they measured an exciton diffusivity of 0.3 cm² s⁻¹, but at higher fluence, they observed a halo effect, wherein the PL intensity at the center of the image was actually lower than at the edges of the image (**Figure 7c**). This behavior seems to indicate some memory of prior excitation events or past excitation density and may arise from temperature gradients or long-lived trapped charge carriers, which can act as nonradiative recombination centers through Auger processes.

3.4.2. The search for intrinsic behavior. Despite experimental successes, it is clear that defects dominate many experimental observations of exciton transport in TMDs (40, 41, 53, 163, 164). This assertion is supported by recent reports of dramatically narrower PL linewidths when TMDs are encapsulated in hexagonal boronitride, suggesting that excitonic states in previously studied materials are strongly inhomogeneously broadened (165, 166). Such high-quality materials may be required before more elusive intrinsic effects like anisotropic and valley-dependent transport can be observed (167, 168) (see the sidebar titled Valleytronics in Two-Dimensional Transition Metal Dichalcogenides).

4. OUTLOOK: THE PRESENT AND FUTURE OF SPATIOTEMPORALLY RESOLVED ENERGY FLOW

The high-resolution spatiotemporally resolved approaches discussed in this review are well suited to elucidate energy transport in emerging semiconductors, whose transport mechanisms' spatiotemporal heterogeneities are not well characterized by conventional semiconductor measurements. By directly resolving the rate of energy flow as a function of space and time rather than more traditionally measuring the extent of travel over an energy carrier's lifetime, these approaches reveal a rich set of deviations from normal diffusion and the mechanisms by which

VALLEYTRONICS IN TWO-DIMENSIONAL TRANSITION METAL DICHALCOGENIDES

Excitons and free charge carriers in noncentrosymmetric transition metal dichalcogenides (TMDs) possess an additional degree of freedom associated with the particular valley of the electronic band structure into which they were initially excited (181). Excitons are described using an additional valley index of +K or -K, and populations of a given index can be selectively excited using circularly polarized light (182–184). Manifestations of this unique behavior include the valley Hall effect (185, 186) and electrically driven generation of circularly polarized light using valley-polarized excitons (187). The emerging field of valleytronics seeks to manipulate and leverage valley index information analogous to the spin degree of freedom in spintronics (181). Interestingly, valley-dependent excitation is predicted to lead to anisotropic transport in some TMDs (167, 168).

structural features determine functional properties. In fact, the introduction of spatial information through these measurements is prompting the field to develop new vocabulary to describe electronic energy transport, especially in materials in which the more traditional parameter L_D is comparable to scales of morphological heterogeneity. These techniques enable intrinsic semiconductor properties to be measured locally in both space and time, much in the way that single-molecule spectroscopy characterizes distributions in addition to mean parameter values. Moreover, this aspect has allowed traditional transport parameters like diffusivity, scattering time, or hopping rates to be obtained selectively in regions of space-time in which they are constant.

It is interesting to note that no one spatiotemporal approach is currently able to span the broad dynamic range in time delay and resolution required to achieve a holistic picture of energy transport dynamics. It is in fact only by assembling the results from all spatiotemporal approaches that we have captured a more complete picture that spans early-time, superdiffusive unthermalized behavior; moderate-time diffusive behavior within locally homogeneous volumes; and longer-time subdiffusive, or more correctly, nonequilibrium, dynamics due to spatioenergetic inhomogeneities. We have also established how different forms of dynamic microscopy have complementarities beyond temporal range and resolution, including excited species selectivity, detection sensitivity and speed, dimensionality, and direct readout versus reliance on modeling. No doubt, coordinating efforts in the future will allow the field to address progressively more challenging materials problems. Furthermore, additional synergistic, technical advances could enable us to better specify the structure-function relationships in emerging materials, be they in light source, imaging, or detector technology, or in advanced algorithms for data acquisition and analysis. In particular, methods to more directly correlate the functional imaging at the heart of this review with both in situ and ex situ structural maps possessing resolution on the scales of structural and dynamic heterogeneity will provide the ultimate tool to facilitate breakthroughs not only in fundamental science but also in the device technologies associated with emerging semiconductors.

DISCLOSURE STATEMENT

The authors are not aware of any affiliations, memberships, funding, or financial holdings that might be perceived as affecting the objectivity of this review.

ACKNOWLEDGMENTS

W.A.T. acknowledges support from the US Department of Energy, Office of Science, Office of Basic Energy Sciences (awards DE-SC0001088 and DE-SC0019345). W.A.T. also acknowledges help from Kristopher Williams in generating figures. N.S.G. acknowledges support from the Science and Technology Center on Real-Time Functional Imaging, a National Science Foundation Science and Technology Center (grant DMR 1548924), the Dow Chemical Company (contract 244699), the Photonics at Thermodynamic Limits' Energy Frontier Research Center funded by the US Department of Energy, Office of Science, Office of Basic Energy Sciences (award DE-SC0019140), a David and Lucile Packard Fellowship for Science and Engineering, an Alfred P. Sloan Research Fellowship, and a Camille Dreyfus Teacher-Scholar Award. N.S.G. also extends her gratitude to Milan Delor for constructive feedback on the manuscript.

LITERATURE CITED

1. Nomura K, Ohta H, Takagi A, Kamiya T, Hirano M, Hosono H. 2004. Room-temperature fabrication of transparent flexible thin-film transistors using amorphous oxide semiconductors. *Nature* 432(7016):488–92

2. Chang J-F, Sakanoue T, Olivier Y, Uemura T, Dufourg-Madec M-B, et al. 2011. Hall-effect measurements probing the degree of charge-carrier delocalization in solution-processed crystalline molecular semiconductors. *Phys. Rev. Lett.* 107(6):066601
3. Zhang Y, Ye J, Matsuhashi Y, Iwasa Y. 2012. Ambipolar MoS₂ thin flake transistors. *Nano Lett.* 12(3):1136–40
4. Stoumpos CC, Malliakas CD, Kanatzidis MG. 2013. Semiconducting tin and lead iodide perovskites with organic cations: phase transitions, high mobilities, and near-infrared photoluminescent properties. *Inorg. Chem.* 52(15):9019–38
5. Hoofman R, de Haas MP, Siebbeles LDA, Warman JM. 1998. Highly mobile electrons and holes on isolated chains of the semiconducting polymer poly(phenylenevinylene). *Nature* 392(6671):54–56
6. Lee JS, Kovalenko MV, Huang J, Chung DS, Talapin DV. 2011. Band-like transport, high electron mobility and high photoconductivity in all-inorganic nanocrystal arrays. *Nat. Nanotechnol.* 6(6):348–52
7. Savenije TJ, Ferguson AJ, Kopidakis N, Rumbles G. 2013. Revealing the dynamics of charge carriers in polymer:fullerene blends using photoinduced time-resolved microwave conductivity. *J. Phys. Chem. C* 117(46):24085–103
8. Ponseca CS, Savenije TJ, Abdellah M, Zheng K, Yartsev A, et al. 2014. Organometal halide perovskite solar cell materials rationalized: ultrafast charge generation, high and microsecond-long balanced mobilities, and slow recombination. *J. Am. Chem. Soc.* 136(14):5189–92
9. Salcedo JR, Siegman AE, Dlott DD, Fayer MD. 1978. Dynamics of energy transport in molecular crystals: the picosecond transient-grating method. *Phys. Rev. Lett.* 41(2):131–34
10. Lloyd-Hughes J, Jeon T-I. 2012. A review of the terahertz conductivity of bulk and nano-materials. *J. Infrared Millim. Terahertz Waves* 33(9):871–925
11. Ulbricht R, Hendry E, Shan J, Heinz TF, Bonn M. 2011. Carrier dynamics in semiconductors studied with time-resolved terahertz spectroscopy. *Rev. Mod. Phys.* 83(2):543–86
12. Yettapu GR, Talukdar D, Sarkar S, Swarnkar A, Nag A, et al. 2016. Terahertz conductivity within colloidal CsPbBr₃ perovskite nanocrystals: remarkably high carrier mobilities and large diffusion lengths. *Nano Lett.* 16(8):4838–48
13. Gilmore RH, Lee EMY, Weidman MC, Willard AP, Tisdale WA. 2017. Charge carrier hopping dynamics in homogeneously broadened PbS quantum dot solids. *Nano Lett.* 17(2):893–901
14. Guzelurk B, Belisle RA, Smith MD, Bruening K, Prasanna R, et al. 2018. Terahertz emission from hybrid perovskites driven by ultrafast charge separation and strong electron–phonon coupling. *Adv. Mater.* 30(11):1704737
15. Bischak CG, Sanehira EM, Precht JT, Luther JM, Ginsberg NS. 2015. Heterogeneous charge carrier dynamics in organic-inorganic hybrid materials: nanoscale lateral and depth-dependent variation of recombination rates in methylammonium lead halide perovskite thin films. *Nano Lett.* 15(7):4799–807
16. Haegel NM, Ke C, Taha H, Guthrey H, Fetzer CM, King RR. 2017. Cross-sectional transport imaging in a multijunction solar cell. *IEEE J. Photovolt.* 7(1):354–58
17. Shaw PE, Ruseckas A, Samuel IDW. 2008. Exciton diffusion measurements in poly(3-hexylthiophene). *Adv. Mater.* 20(18):3516–20
18. Markov DE, Amsterdam E, Blom PWM, Sieval AB, Hummelen JC. 2005. Accurate measurement of the exciton diffusion length in a conjugated polymer using a heterostructure with a side-chain cross-linked fullerene layer. *J. Phys. Chem. A* 109(24):5266–74
19. Scully SR, McGehee MD. 2006. Effects of optical interference and energy transfer on exciton diffusion length measurements in organic semiconductors. *J. Appl. Phys.* 100(3):034907
20. Lunt RR, Giebink NC, Belak AA, Benziger JB, Forrest SR. 2009. Exciton diffusion lengths of organic semiconductor thin films measured by spectrally resolved photoluminescence quenching. *J. Appl. Phys.* 105(5):053711
21. Stranks SD, Eperon GE, Grancini G, Menelaou C, Alcocer MJP, et al. 2013. Electron-hole diffusion lengths exceeding 1 micrometer in an organometal trihalide perovskite absorber. *Science* 342(6156):341–44

22. Menke SM, Holmes RJ. 2014. Exciton diffusion in organic photovoltaic cells. *Energy Environ. Sci.* 7(2):499–512
23. Mikhnenko O, Blom P, Nguyen T-QT. 2015. Exciton diffusion in organic semiconductors. *Energy Environ. Sci.* 8(7):1867–88
24. Lee EMY, Tisdale WA. 2015. Determination of exciton diffusion length by transient photoluminescence quenching and its application to quantum dot films. *J. Phys. Chem. C* 119(17):9005–15
25. Dong Q, Fang Y, Shao Y, Mulligan P, Qiu J, et al. 2015. Electron-hole diffusion lengths >175 μm in solution-grown $\text{CH}_3\text{NH}_3\text{PbI}_3$ single crystals. *Science* 347(6225):967–70
26. Kholmicheva N, Moroz P, Bastola E, Razgoniaeva N, Bocanegra J, et al. 2015. Mapping the exciton diffusion in semiconductor nanocrystal solids. *ACS Nano.* 9(3):2926–37
27. Fleming GR, van Grondelle R. 1997. Femtosecond spectroscopy of photosynthetic light-harvesting systems. *Curr. Opin. Struct. Biol.* 7(5):738–48
28. Pullerits T, Sundström V. 1996. Photosynthetic light-harvesting pigment–protein complexes: toward understanding how and why. *Acc. Chem. Res.* 29(8):381–89
29. Cheng Y-C, Fleming GR. 2009. Dynamics of light harvesting in photosynthesis. *Annu. Rev. Phys. Chem.* 60(1):241–62
30. Ginsberg NS, Cheng Y-C, Fleming GR. 2009. Two-dimensional electronic spectroscopy of molecular aggregates. *Acc. Chem. Res.* 42(9):1352–63
31. Alivisatos AP. 1996. Semiconductor clusters, nanocrystals, and quantum dots. *Science* 271(5251):933–37
32. Klimov VI. 2000. Optical nonlinearities and ultrafast carrier dynamics in semiconductor nanocrystals. *J. Phys. Chem. B* 104(26):6112–23
33. Bawendi MG, Steigerwald ML, Brus LE. 1990. The quantum mechanics of larger semiconductor clusters (quantum dots). *Annu. Rev. Phys. Chem.* 41:477–96
34. Akselrod GM, Prins F, Poulidakos LV, Lee EMY, Weidman MC, et al. 2014. Subdiffusive exciton transport in quantum dot solids. *Nano Lett.* 14:3556–62
35. Akselrod GM, Deotare PB, Thompson NJ, Lee J, Tisdale WA, et al. 2014. Visualization of exciton transport in ordered and disordered molecular solids. *Nat. Commun.* 5:3646
36. Delor M, Weaver HL, Yu Q, Ginsberg NS. 2020. Imaging material functionality through three-dimensional nanoscale tracking of energy flow. *Nat. Mater.* 19:56–62
37. Penwell SB, Ginsberg LDS, Ginsberg NS. 2015. Bringing far-field subdiffraction optical imaging to electronically coupled optoelectronic molecular materials using their endogenous chromophores. *J. Phys. Chem. Lett.* 6(14):2767–72
38. Grumstrup EM, Gabriel MM, Cating EEM, Van Goethem EM, Papanikolas JM. 2015. Pump-probe microscopy: visualization and spectroscopy of ultrafast dynamics at the nanoscale. *Chem. Phys.* 458:30–40
39. Guo Z, Wan Y, Yang M, Snaider J, Zhu K, Huang L. 2017. Long-range hot-carrier transport in hybrid perovskites visualized by ultrafast microscopy. *Science* 356(6333):59–62
40. Yuan L, Wang T, Zhu T, Zhou M, Huang L. 2017. Exciton dynamics, transport, and annihilation in atomically thin two-dimensional semiconductors. *J. Phys. Chem. Lett.* 8(14):3371–79
41. Kulig M, Zipfel J, Nagler P, Blanter S, Schüller C, et al. 2018. Exciton diffusion and halo effects in monolayer semiconductors. *Phys. Rev. Lett.* 120(20):207401
42. Wan Y, Guo Z, Zhu T, Yan S, Johnson J, Huang L. 2015. Cooperative singlet and triplet exciton transport in tetracene crystals visualized by ultrafast microscopy. *Nat. Chem.* 7(10):785–92
43. Zhu T, Wan Y, Guo Z, Johnson J, Huang L. 2016. Two birds with one stone: tailoring singlet fission for both triplet yield and exciton diffusion length. *Adv. Mater.* 28(34):7539–47
44. Penwell SB, Ginsberg LDS, Noriega R, Ginsberg NS. 2017. Resolving ultrafast exciton migration in organic solids at the nanoscale. *Nat. Mater.* 16(11):1136–41
45. Zhu T, Wan Y, Huang L. 2017. Direct imaging of Frenkel exciton transport by ultrafast microscopy. *Acc. Chem. Res.* 50(7):1725–33
46. Wan Y, Stradomska A, Knoester J, Huang L. 2017. Direct imaging of exciton transport in tubular porphyrin aggregates by ultrafast microscopy. *J. Am. Chem. Soc.* 139(21):7287–93

47. Yoon SJ, Guo Z, dos Santos Claro PC, Shevchenko EV, Huang L. 2016. Direct imaging of long-range exciton transport in quantum dot superlattices by ultrafast microscopy. *ACS Nano*. 10(7):7208–15
48. Guo Z, Manser JS, Wan Y, Kamat PV, Huang L. 2015. Spatial and temporal imaging of long-range charge transport in perovskite thin films by ultrafast microscopy. *Nat. Commun.* 6:7471
49. Kennedy CL, Hill AH, Massaro ES, Grumstrup EM. 2017. Ultrafast excited-state transport and decay dynamics in cesium lead mixed halide perovskites. *ACS Energy Lett.* 2(7):1501–6
50. Hill AH, Smyser KE, Kennedy CL, Massaro ES, Grumstrup EM. 2017. Screened charge carrier transport in methylammonium lead iodide perovskite thin films. *J. Phys. Chem. Lett.* 8(5):948–53
51. Hill AH, Kennedy CL, Massaro ES, Grumstrup EM. 2018. Perovskite carrier transport: disentangling the impacts of effective mass and scattering time through microscopic optical detection. *J. Phys. Chem. Lett.* 9(11):2808–13
52. Snaider JM, Guo Z, Wang T, Yang M, Yuan L, et al. 2018. Ultrafast imaging of carrier transport across grain boundaries in hybrid perovskite thin films. *ACS Energy Lett.* 3(6):1402–8
53. Goodman AJ, Lien D-H, Ahn GH, Spiegel LL, Amani M, et al. 2018. Suppressing diffusion-mediated exciton annihilation in 2D semiconductors using the dielectric environment. arXiv:1811.01066 [cond-mat.mtrl-sci]
54. Gabriel MM, Kirschbrown JR, Christesen JD, Pinion CW, Zigler DF, et al. 2013. Direct imaging of free carrier and trap carrier motion in silicon nanowires by spatially-separated femtosecond pump-probe microscopy. *Nano Lett.* 13(3):1336–40
55. Scholes GD. 2003. Long-range resonance energy transfer in molecular systems. *Annu. Rev. Phys. Chem.* 54(1):57–87
56. Scholes GD, Rumbles G. 2006. Excitons in nanoscale systems. *Nat. Mater.* 5(9):683–96
57. Köhler A, Bässler H. *Electronic Processes in Organic Semiconductors: An Introduction*. Weinheim, Ger.: Wiley-VCH
58. Kasha M. 1963. Energy transfer mechanisms and the molecular exciton model for molecular aggregates. *Radiat. Res.* 20(1):55–70
59. Davydov AS. 1964. The theory of molecular excitons. *Sov. Phys. Uspekhi.* 7(2):145
60. Kayanuma Y. 1986. Wannier exciton in microcrystals. *Solid State Commun.* 59(6):405–8
61. Hsu C-P. 2009. The electronic couplings in electron transfer and excitation energy transfer. *Acc. Chem. Res.* 42(4):509–18
62. Troisi A. 2011. Charge transport in high mobility molecular semiconductors: classical models and new theories. *Chem. Soc. Rev.* 40(5):2347–58
63. Aragón J, Troisi A. 2015. Dynamics of the excitonic coupling in organic crystals. *Phys. Rev. Lett.* 114(2):026402
64. Rivas Á, Huelga SF, Plenio MB. 2014. Quantum non-Markovianity: characterization, quantification and detection. *Rep. Prog. Phys.* 77(9):094001
65. Chenu A, Scholes GD. 2015. Coherence in energy transfer and photosynthesis. *Annu. Rev. Phys. Chem.* 66:69–96
66. Barford W, Tozer OR. 2014. Theory of exciton transfer and diffusion in conjugated polymers. *J. Chem. Phys.* 141(16):164103
67. Marcus RA. 1993. Electron transfer reactions in chemistry. Theory and experiment. *Rev. Mod. Phys.* 65(3):599–610
68. Förster T. 1948. Zwischenmolekulare Energiewanderung und Fluoreszenz. *Ann. Phys.* 437(1–2):55–75
69. Dexter DL. 1953. A theory of sensitized luminescence in solids. *J. Chem. Phys.* 21(5):836–50
70. Grover M, Silbey R. 1971. Exciton migration in molecular crystals. *J. Chem. Phys.* 54(11):4843–51
71. Coropceanu V, Cornil J, da Silva Filho DA, Olivier Y, Silbey R, Brédas J-L. 2007. Charge transport in organic semiconductors. *Chem. Rev.* 107(4):926–52
72. Ishizaki A, Fleming GR. 2009. Unified treatment of quantum coherent and incoherent hopping dynamics in electronic energy transfer: reduced hierarchy equation approach. *J. Chem. Phys.* 130(23):234111
73. Sakanoue T, Siringhaus H. 2010. Band-like temperature dependence of mobility in a solution-processed organic semiconductor. *Nat. Mater.* 9(9):736–40

74. Wang L, Beljonne D. 2013. Flexible surface hopping approach to model the crossover from hopping to band-like transport in organic crystals. *J. Phys. Chem. Lett.* 4(11):1888–94
75. Noriega R, Rivnay J, Vandewal K, Koch FPV, Stingelin N, et al. 2013. A general relationship between disorder, aggregation and charge transport in conjugated polymers. *Nat. Mater.* 12(11):1038–44
76. Rozenman GG, Akulov K, Golombek A, Schwartz T. 2018. Long-range transport of organic exciton-polaritons revealed by ultrafast microscopy. *ACS Photon.* 5(1):105–10
77. Lindfors K, Kalkbrenner T, Stoller P, Sandoghdar V. 2004. Detection and spectroscopy of gold nanoparticles using supercontinuum white light confocal microscopy. *Phys. Rev. Lett.* 93(3):037401
78. Jacobsen V, Stoller P, Brunner C, Vogel V, Sandoghdar V. 2006. Interferometric optical detection and tracking of very small gold nanoparticles at a water-glass interface. *Opt. Express* 14(1):405–14
79. Piliarik M, Sandoghdar V. 2014. Direct optical sensing of single unlabelled proteins and super-resolution imaging of their binding sites. *Nat. Commun.* 5:4495
80. Young G, Hundt N, Cole D, Fineberg A, Andrecka J, et al. 2018. Quantitative mass imaging of single biological macromolecules. *Science* 360(6387):423–27
81. Krishnan M, Mojarad N, Kukura P, Sandoghdar V. 2010. Geometry-induced electrostatic trapping of nanometric objects in a fluid. *Nature* 467(7316):692–95
82. Coffey DC, Reid OG, Rodovsky DB, Bartholomew GP, Ginger DS. 2007. Mapping local photocurrents in polymer/fullerene solar cells with photoconductive atomic force microscopy. *Nano Lett.* 7(3):738–44
83. Bao W, Melli M, Caselli N, Riboli F, Wiersma DS, et al. 2012. Mapping local charge recombination heterogeneity by multidimensional nanospectroscopic imaging. *Science* 338(6112):1317–21
84. Atkin JM, Berweger S, Jones AC, Raschke MB. 2012. Nano-optical imaging and spectroscopy of order, phases, and domains in complex solids. *Adv. Phys.* 61(6):745–842
85. de Quilettes DW, Vorpahl SM, Stranks SD, Nagaoka H, Eperon GE, et al. 2015. Impact of microstructure on local carrier lifetime in perovskite solar cells. *Science* 348(6235):683–86
86. Pierret RF. 1988. *Semiconductor Fundamentals*, Vol. I. Reading, MA: Addison-Wesley. 2nd ed.
87. Brédas J-L, Sargent EH, Scholes GD. 2017. Photovoltaic concepts inspired by coherence effects in photosynthetic systems. *Nat. Mater.* 16(1):35–44
88. Scholes GD, Fleming GR, Chen LX, Aspuru-Guzik A, Buchleitner A, et al. 2017. Using coherence to enhance function in chemical and biophysical systems. *Nature* 543(7647):647–56
89. Rose TS, Righini R, Fayer MD. 1984. Picosecond transient grating measurements of singlet exciton transport in anthracene single crystals. *Chem. Phys. Lett.* 106(1):13–19
90. Müller AM, Bardeen CJ. 2007. Using a streak camera to resolve the motion of molecular excited states with picosecond time resolution and 150 nm spatial resolution. *J. Phys. Chem. C.* 111(33):12483–89
91. Avakian P, Merrifield RE. 1968. Triplet excitons in anthracene crystals—a review. *Mol. Cryst.* 5(1):37–77
92. Adams DM, Kerimo J, O’Connor DB, Barbara PF. 1999. Spatial imaging of singlet energy migration in perylene bis(phenethylimide) thin films. *J. Phys. Chem. A* 103(49):10138–43
93. Irkhin P, Biaggio I. 2011. Direct imaging of anisotropic exciton diffusion and triplet diffusion length in rubrene single crystals. *Phys. Rev. Lett.* 107(1):017402
94. Yuan L, Chung T-F, Kuc A, Wan Y, Xu Y, et al. 2018. Photocarrier generation from interlayer charge-transfer transitions in WS₂-graphene heterostructures. *Sci. Adv.* 4(2):e1700324
95. Prins F, Goodman AJ, Tisdale WA. 2014. Reduced dielectric screening and enhanced energy transfer in single- and few-layer MoS₂. *Nano Lett.* 14(11):6087–91
96. Zhu T, Yuan L, Zhao Y, Zhou M, Wan Y, et al. 2018. Highly mobile charge-transfer excitons in two-dimensional WS₂/tetracene heterostructures. *Sci. Adv.* 4(1):eaa03104
97. Deotare PB, Chang W, Hontz E, Congreve DN, Shi L, et al. 2015. Nanoscale transport of charge-transfer states in organic donor-acceptor blends. *Nat. Mater.* 14(11):1130–34
98. Talapin DV, Lee JS, Kovalenko MV, Shevchenko EV. 2010. Prospects of colloidal nanocrystals for electronic and optoelectronic applications. *Chem. Rev.* 110(1):389–458
99. Kovalenko MV, Protesescu L, Bodnarchuk MI. 2017. Properties and potential optoelectronic applications of lead halide perovskite nanocrystals. *Science* 358(6364):745
100. Bourzac K. 2013. Quantum dots go on display. *Nature* 493(7432):283

101. Carey GH, Abdelhady AL, Ning Z, Thon SM, Bakr OM, Sargent EH. 2015. Colloidal quantum dot solar cells. *Chem. Rev.* 115(23):12732–63
102. Shirasaki Y, Supran GJ, Bawendi MG, Bulović V. 2013. Emergence of colloidal quantum-dot light-emitting technologies. *Nat. Photon.* 7(1):13–23
103. Shevchenko EV, Talapin DV, Kotov NA, O'Brien S, Murray CB. 2006. Structural diversity in binary nanoparticle superlattices. *Nature* 439(7072):55–59
104. Murray CB, Kagan CR, Bawendi MG. 1995. Self-organization of CdSe nanocrystallites into three-dimensional quantum dot superlattices. *Science* 270(5240):1335–38
105. Guyot-Sionnest P. 2012. Electrical transport in colloidal quantum dot films. *J. Phys. Chem. Lett.* 3(9):1169–75
106. Kagan C, Murray C, Nirmal M, Bawendi M. 1996. Electronic energy transfer in CdSe quantum dot solids. *Phys. Rev. Lett.* 76(9):1517–20
107. Crooker SA, Hollingsworth JA, Tretiak S, Klimov VI. 2002. Spectrally resolved dynamics of energy transfer in quantum-dot assemblies: towards engineered energy flows in artificial materials. *Phys. Rev. Lett.* 89(18):186802
108. Lee EMY, Tisdale WA, Willard AP. 2015. Can disorder enhance incoherent exciton diffusion? *J. Phys. Chem. B* 119(30):9501–9
109. Lee EMY, Tisdale WA, Willard AP. 2018. Nonequilibrium dynamics of localized and delocalized excitons in colloidal quantum dot solids. *J. Vac. Sci. Technol. A* 36:068501
110. Kodaimati MS, Wang C, Chapman C, Schatz GC, Weiss EA. 2017. Distance-dependence of interparticle energy transfer in the near-infrared within electrostatic assemblies of PbS quantum dots. *ACS Nano* 11(5):5041–50
111. Azzaro MS, Dodin A, Zhang DY, Willard AP, Roberts ST. 2018. Exciton-delocalizing ligands can speed up energy migration in nanocrystal solids. *Nano Lett.* 18(5):3259–70
112. Frederick MT, Weiss EA. 2010. Relaxation of exciton confinement in CdSe quantum dots by modification with a conjugated dithiocarbamate ligand. *ACS Nano* 4(6):3195–200
113. Reich KV, Shklovskii BI. 2016. Exciton transfer in array of epitaxially connected nanocrystals. *ACS Nano* 10(11):10267–74
114. Pope M, Swenberg CE. 1999. *Electronic Processes in Organic Crystals and Polymers*. Oxford, UK: Oxford Univ. Press. 2nd ed.
115. Bardeen CJ. 2014. The structure and dynamics of molecular excitons. *Annu. Rev. Phys. Chem.* 65:127–48
116. Anthony JE. 2006. Functionalized acenes and heteroacenes for organic electronics. *Chem. Rev.* 106(12):5028–48
117. Zhan X, Facchetti A, Barlow S, Marks TJ, Ratner MA, et al. 2011. Rylene and related diimides for organic electronics. *Adv. Mater.* 23(2):268–84
118. Brédas J-L, Beljonne D, Coropceanu V, Cornil J. 2004. Charge-transfer and energy-transfer processes in π -conjugated oligomers and polymers: a molecular picture. *Chem. Rev.* 104(11):4971–5004
119. Krueger BP, Scholes GD, Fleming GR. 1998. Calculation of couplings and energy-transfer pathways between the pigments of LH2 by the ab initio transition density cube method. *J. Phys. Chem. B* 102(27):5378–86
120. Beljonne D, Cornil J, Silbey R, Millié P, Brédas JL. 2000. Interchain interactions in conjugated materials: the exciton model versus the supermolecular approach. *J. Chem. Phys.* 112(10):4749–58
121. Beenken WJD, Pullerits T. 2004. Excitonic coupling in polythiophenes: comparison of different calculation methods. *J. Chem. Phys.* 120(5):2490–95
122. Beljonne D, Pourtois G, Silva C, Hennebicq E, Herz LM, et al. 2002. Interchain versus intrachain energy transfer in acceptor-capped conjugated polymers. *PNAS* 99(17):10982–87
123. Beljonne D, Curutchet C, Scholes GD, Silbey R. 2009. Beyond Förster resonance energy transfer in biological and nanoscale systems. *J. Phys. Chem. B* 113(19):6583–99
124. Lee J, Jadhav P, Reuswig PD, Yost SR, Thompson NJ, et al. 2013. Singlet exciton fission photovoltaics. *Acc. Chem. Res.* 46(6):1300–11
125. Smith MB, Michl J. 2013. Recent advances in singlet fission. *Annu. Rev. Phys. Chem.* 64:361–86

126. Burdett JJ, Bardeen CJ. 2013. The dynamics of singlet fission in crystalline tetracene and covalent analogs. *Acc. Chem. Res.* 46(6):1312–20
127. Chan W-L, Berkelbach TC, Provorse MR, Monahan NR, Tritsch JR, et al. 2013. The quantum coherent mechanism for singlet fission: experiment and theory. *Acc. Chem. Res.* 46(6):1321–29
128. Wilson MWB, Rao A, Ehrler B, Friend RH. 2013. Singlet exciton fission in polycrystalline pentacene: from photophysics toward devices. *Acc. Chem. Res.* 46(6):1330–38
129. Berkelbach TC, Hybertsen MS, Reichman DR. 2013. Microscopic theory of singlet exciton fission. I. General formulation. *J. Chem. Phys.* 138(11):114102
130. Groff RP, Avakian P, Merrifield RE. 1970. Coexistence of exciton fission and fusion in tetracene crystals. *Phys. Rev. B* 1(2):815–17
131. Hell SW, Wichmann J. 1994. Breaking the diffraction resolution limit by stimulated emission: stimulated-emission-depletion fluorescence microscopy. *Opt. Lett.* 19(11):780–82
132. Massaro ES, Hill AH, Grumstrup EM. 2016. Super-resolution structured pump-probe microscopy. *ACS Photon.* 3(4):501–6
133. Massaro ES, Grumstrup EM. 2017. Label-free saturated structured excitation microscopy. *Photonics* 4(2):36
134. King JT, Granick S. 2016. Operating organic light-emitting diodes imaged by super-resolution spectroscopy. *Nat. Commun.* 7:11691
135. Buttafava M, Boso G, Ruggeri A, Mora AD, Tosi A. 2014. Time-gated single-photon detection module with 110 ps transition time and up to 80 MHz repetition rate. *Rev. Sci. Instrum.* 85(8):083114
136. Green MA, Ho-Baillie A, Snaith HJ. 2014. The emergence of perovskite solar cells. *Nat. Photonics.* 8(7):506–14
137. Gottesman R, Zaban A. 2016. Perovskites for photovoltaics in the spotlight: photoinduced physical changes and their implications. *Acc. Chem. Res.* 49(2):320–29
138. Brenner TM, Egger DA, Kronik L, Hodes G, Cahen D. 2016. Hybrid organic—inorganic perovskites: low-cost semiconductors with intriguing charge-transport properties. *Nat. Rev. Mater.* 1(1):15007
139. Correa-Baena J-P, Abate A, Saliba M, Tress W, Jacobsson TJ, et al. 2017. The rapid evolution of highly efficient perovskite solar cells. *Energy Environ. Sci.* 10(3):710–27
140. Jeon NJ, Noh JH, Yang WS, Kim YC, Ryu S, et al. 2015. Compositional engineering of perovskite materials for high-performance solar cells. *Nature* 517(7535):476–80
141. Li W, Wang Z, Deschler F, Gao S, Friend RH, Cheetham AK. 2017. Chemically diverse and multifunctional hybrid organic-inorganic perovskites. *Nat. Rev. Mater.* 2(3):16099
142. Petrus ML, Schlipf J, Li C, Gujar TP, Giesbrecht N, et al. 2017. Capturing the sun: a review of the challenges and perspectives of perovskite solar cells. *Adv. Energy Mater.* 7(16):1700264
143. Berry J, Buonassisi T, Egger DA, Hodes G, Kronik L, et al. 2015. Hybrid organic-inorganic perovskites (HOIPs): opportunities and challenges. *Adv. Mater.* 27(35):5102–12
144. Leblebici SY, Leppert L, Li Y, Reyes-Lillo SE, Wickenburg S, et al. 2016. Facet-dependent photovoltaic efficiency variations in single grains of hybrid halide perovskite. *Nat. Energy* 1(8):16093
145. Ball JM, Petrozza A. 2016. Defects in perovskite-halides and their effects in solar cells. *Nat. Energy* 1(11):16149
146. Correa-Baena J-P, Saliba M, Buonassisi T, Grätzel M, Abate A, et al. 2017. Promises and challenges of perovskite solar cells. *Science* 358(6364):739–44
147. Manser JS, Kamat PV. 2014. Band filling with free charge carriers in organometal halide perovskites. *Nat. Photon.* 8(9):737–43
148. MacDonald GA, Yang M, Berweger S, Killgore JP, Kabos P, et al. 2016. Methylammonium lead iodide grain boundaries exhibit depth-dependent electrical properties. *Energy Environ. Sci.* 9(12):3642–49
149. Mak KF, Lee C, Hone J, Shan J, Heinz TF. 2010. Atomically thin MoS₂: a new direct-gap semiconductor. *Phys. Rev. Lett.* 105:136805
150. Radisavljevic B, Radenovic A, Brivio J, Giacometti V, Kis A. 2011. Single-layer MoS₂ transistors. *Nat. Nanotechnol.* 6:147–50
151. Sundaram RS, Engel M, Lombardo A, Krupke R, Ferrari AC, et al. 2013. Electroluminescence in single layer MoS₂. *Nano Lett.* 13(4):1416–21

152. Wu S, Buckley S, Schaibley JR, Feng L, Yan J, et al. 2015. Monolayer semiconductor nanocavity lasers with ultralow thresholds. *Nature* 520(7545):69–72
153. Liu X, Galfsky T, Sun Z, Xia F, Lin E, et al. 2014. Strong light-matter coupling in two-dimensional atomic crystals. *Nat. Photon.* 9:30
154. Chernikov A, Berkelbach TC, Hill HM, Rigosi A, Li Y, et al. 2014. Exciton binding energy and nonhydrogenic Rydberg series in monolayer WS₂. *Phys. Rev. Lett.* 113:076802
155. Hill HM, Rigosi AF, Roquelet C, Chernikov A, Berkelbach TC, et al. 2015. Observation of excitonic Rydberg states in monolayer MoS₂ and WS₂ by photoluminescence excitation spectroscopy. *Nano Lett.* 15(5):2992–97
156. Zhu B, Chen X, Cui X. 2015. Exciton binding energy of monolayer WS₂. *Sci. Rep.* 5:9218
157. Lin Y, Ling X, Yu L, Huang S, Hsu AL, et al. 2014. Dielectric screening of excitons and trions in single-layer MoS₂. *Nano Lett.* 14(10):5569–76
158. Hong X, Kim J, Shi S-F, Zhang Y, Jin C, et al. 2014. Ultrafast charge transfer in atomically thin MoS₂/WS₂ heterostructures. *Nat. Nanotechnol.* 9:682–86
159. Mayers ZM, Berkelbach TC, Hybertsen MS, Reichman DR. 2015. Binding energies and spatial structures of small carrier complexes in monolayer transition-metal dichalcogenides via diffusion Monte Carlo. *Phys. Rev. B* 92:161404
160. You Y, Zhang X-X, Berkelbach TC, Hybertsen MS, Reichman DR, Heinz TF. 2015. Observation of biexcitons in monolayer WSe₂. *Nat. Phys.* 11:477–81
161. Atallah TL, Wang J, Bosch M, Seo D, Burke RA, et al. 2017. Electrostatic screening of charged defects in monolayer MoS₂. *J. Phys. Chem. Lett.* 8(10):2148–52
162. Amani M, Lien D-H, Kiriya D, Xiao J, Azcatl A, et al. 2015. Near-unity photoluminescence quantum yield in MoS₂. *Science* 350(6264):1065–68
163. Goodman AJ, Willard AP, Tisdale WA. 2017. Exciton trapping is responsible for the long apparent lifetime in acid-treated MoS₂. *Phys. Rev. B* 96(12):121404
164. Kato T, Kaneko T. 2016. Transport dynamics of neutral excitons and trions in monolayer WS₂. *ACS Nano* 10(10):9687–94
165. Cadiz F, Courtade E, Robert C, Wang G, Shen Y, et al. 2017. Excitonic linewidth approaching the homogeneous limit in MoS₂-based van der Waals heterostructures. *Phys. Rev. X* 7(2):021026
166. Obafunso AA, Jenny VA, Gabriella DS, Jue W, Abhinandan A, et al. 2017. Approaching the intrinsic photoluminescence linewidth in transition metal dichalcogenide monolayers. *2D Mater.* 4(3):031011
167. Ghazaryan A, Hafezi M, Ghaemi P. 2018. Anisotropic exciton transport in transition-metal dichalcogenides. *Phys. Rev. B* 97(24):245411
168. Onga M, Zhang Y, Ideue T, Iwasa Y. 2017. Exciton Hall effect in monolayer MoS₂. *Nat. Mater.* 16(12):1193–97
169. Emin D. 2012. *Polarons*. Cambridge, UK: Cambridge Univ. Press
170. Spano FC. 2010. The spectral signatures of Frenkel polarons in H- and J-aggregates. *Acc. Chem. Res.* 43(3):429–39
171. Miyata K, Atallah TL, Zhu X-Y. 2017. Lead halide perovskites: crystal-liquid duality, phonon glass electron crystals, and large polaron formation. *Sci. Adv.* 3(10):e1701469
172. Bischak CG, Hetherington CL, Wu H, Aloni S, Ogletree DF, et al. 2017. Origin of reversible photoinduced phase separation in hybrid perovskites. *Nano Lett.* 17(2):1028–33
173. Zimmerman PM, Musgrave CB, Head-Gordon M. 2013. A correlated electron view of singlet fission. *Acc. Chem. Res.* 46(6):1339–47
174. Yost SR, Lee J, Wilson MWB, Wu T, McMahon DP, et al. 2014. A transferable model for singlet-fission kinetics. *Nat. Chem.* 6(6):492–97
175. Sanders SN, Kumarasamy E, Pun AB, Trinh MT, Choi B, et al. 2015. Quantitative intramolecular singlet fission in bipentacenes. *J. Am. Chem. Soc.* 137(28):8965–72
176. Korovina NV, Das S, Nett Z, Feng X, Joy J, et al. 2016. Singlet fission in a covalently linked cofacial alkynyltetracene dimer. *J. Am. Chem. Soc.* 138(2):617–27
177. Stern HL, Musser AJ, Gelinas S, Parkinson P, Herz LM, et al. 2015. Identification of a triplet pair intermediate in singlet exciton fission in solution. *PNAS* 112:7656–61

178. Pensack RD, Ostroumov EE, Tilley AJ, Mazza S, Grieco C, et al. 2016. Observation of two triplet-pair intermediates in singlet exciton fission. *J. Phys. Chem. Lett.* 7(13):2370–75
179. Folie BD, Haber JB, Refaely-Abramson S, Neaton JB, Ginsberg NS. 2018. Long-lived correlated triplet pairs in a π -stacked crystalline pentacene derivative. *J. Am. Chem. Soc.* 140(6):2326–35
180. Sharifzadeh S, Wong CY, Wu H, Cotts BL, Kronik L, et al. 2014. Relating the physical structure and optoelectronic function of crystalline TIPS-pentacene. *Adv. Funct. Mater.* 25(13):2038–46
181. Schaibley JR, Yu HY, Clark G, Rivera P, Ross JS, et al. 2016. Valleytronics in 2D materials. *Nat. Rev. Mater.* 1(11):16055
182. Xiao D, Liu G-B, Feng W, Xu X, Yao W. 2012. Coupled spin and valley physics in monolayers of MoS₂ and other group-VI dichalcogenides. *Phys. Rev. Lett.* 108(19):196802
183. Zeng H, Dai J, Yao W, Xiao D, Cui X. 2012. Valley polarization in MoS₂ monolayers by optical pumping. *Nat. Nanotechnol.* 7:490–93
184. Mak KF, He K, Shan J, Heinz TF. 2012. Control of valley polarization in monolayer MoS₂ by optical helicity. *Nat. Nanotechnol.* 7:494–98
185. Mak KF, McGill KL, Park J, McEuen PL. 2014. The valley Hall effect in MoS₂ transistors. *Science* 344(6191):1489–92
186. Lee J, Mak KF, Shan J. 2016. Electrical control of the valley Hall effect in bilayer MoS₂ transistors. *Nat. Nanotechnol.* 11:421–25
187. Zhang YJ, Oka T, Suzuki R, Ye JT, Iwasa Y. 2014. Electrically switchable chiral light-emitting transistor. *Science* 344(6185):725–28